I. APPLICATION OF MULTI-REGGE THEORY TO PRODUCTION PROCESSES

II. HIGH ENERGY MODEL FOR PROTON-PROTON SCATTERING

Thesis by

Richard Gwin Lipes

In Partial Fulfillment of the Requirements

For the Degree of

Doctor of Philosophy

California Institute of Technology

Pasadena, California

1969

(Submitted May 23, 1969)

ACKNOWLEDGMENTS

I wish especially to thank my advisor, Professor George Zweig, for the close association that has, in addition to making this work possible, taught me much about the "art" of physics.

I would also like to thank Professor Loyal Durand III for many illuminating discussions and to acknowledge that the work on proton-proton scattering was done in collaboration with him.

Financial support by the National Science Foundation throughout the course of this work I have greatly appreciated.

ABSTRACT

This dissertation consists of two parts. The first part presents an explicit procedure for applying multi-Regge theory to production processes. As an illustrative example, the case of three body final states is developed in detail, both with respect to kinematics and multi-Regge dynamics. Next, the experimental consistency of the multi-Regge hypothesis is tested in a specific high energy reaction; the hypothesis is shown to provide a good qualitative fit to the data. In addition, the results demonstrate a severe suppression of double Pomeranchon exchange, and show the coupling of two "Reggeons" to an external particle to be strongly damped as the particle's mass increases. Finally, with the use of two body Regge parameters, order of magnitude estimates of the multi-Regge cross section for various reactions are given.

The second part presents a diffraction model for high energy proton-proton scattering. This model developed by Chou and Yang assumes high energy elastic scattering results from absorption of the incident wave into the many available inelastic channels, with the absorption proportional to the amount of interpenetrating hadronic matter. The assumption that the hadronic matter distribution is proportional to the charge distribution relates the scattering amplitude for pp scattering to the proton form factor. The Chou-Yang model with the empirical proton form factor as input is then applied to calculate a high energy, fixed momentum transfer limit for the scattering cross section. This limiting cross section exhibits the same "dip" or "break" structure indicated in present experiments, but falls significantly below them in magnitude. Finally, possible spin dependence is introduced through a weak spin-orbit type term which gives rather good agreement with pp polarization data.

TABLE OF CONTENTS

I. APPLICATION OF MULTI-REGGE THEORY TO PRODUCTION PROCESSES

II. HIGH ENERGY MODEL FOR PROTON-PROTON SCATTERING

I. Application of Multi-Regge Theory to Production Processes

CHAPTER I

Introduction

One of the most striking features of high energy processes is the phenomenon of multi-particle production. Theoretical investigation of the multi-particle production processes began with the work of Amati, Fubini, and Stanghellini (AFS)[1] on "multi-peripheralism." In this work they factor the amplitude into a product of off-mass shell two body amplitudes and connecting propagators, a form following from the assumption that the "most peripheral" graphs dominate. Next, Frautschi[2] emphasized a factorization of multi-particle production amplitudes into two body amplitudes with final state clusters having small invariant masses and strong "damping" in momentum transfer. He assumed exponential damping, whereas, AFS considered a power law damping coming from the propagator. Frautschi noted the desirability of applying Reggeism to production processes, but was unable to formulate a program to this end. This problem was later taken up independently by several authors[3, 4, 5] who assumed that, in certain well-defined kinematic regions, the multi-particle production amplitude factored into a product of two body Regge amplitudes. We will call this the multi-Regge exchange (MRE) hypothesis.

In order to utilize unitarity at high energies, the structure of the multi-particle production amplitude must be known. The primary importance of the MRE hypothesis is that it provides a model for this structure. The multi-Regge cross section for a single reaction may be far below the cross sections for elastic and diffraction dissociation scattering of the same initial particles. Nevertheless,

the total of all multi-Regge contributions may represent a large part of the unitarity sum. Consequently, it is important to check the consistency of the hypothesis and determine the phenomenological parameters of the amplitude. This is the purpose of this work.

In Chapter II, we discuss the kinematics of three body final states. The variables are carefully defined, useful plots are discussed, and derivation of plot boundaries is given. In Chapter III, we develop a program for analyzing multi-Regge events. Choice of contributing trajectories, cuts in the data, and use of distributions are considered. Explicit formulae are given for three body final states. Chapter IV deals with application of the Chapter III program to a particular reaction with emphasis on checking the consistency of the hypothesis. The question of double Pomeranchuk exchange is treated. Finally, in Chapter V we give estimates of multi-Regge cross sections for a set of reactions.

CHAPTER II

Kinematics

A description of any process in which two particles scatter into N particles requires, in general, 3N - 4 independent variables. The N + 2 four vectors represent 3(N + 2) independent components. Invariance of the description under non-homogeneous Lorentz transformations provides ten constraints. Four of these come from translational invariance or energy-momentum conservation. Three come from rotational invariance or angular momentum conservation. The remaining three come from invariance under Lorentz boosts. The detailed form of the dynamics and phase space dictates the utility of the choice of independent variables. For three body final states, pronounced variation of the scattering cross sections in momentum exchange and total energy suggests the usefulness of the variables*

$$t_{12} = (q_1 - q_a)^2,\ t_{23} = (q_3 - q_b)^2,\ s_{12} = (q_1 + q_2)^2,\ s_{23} = (q_2 + q_3)^2,$$

$$s = (q_a + q_b)^2 \qquad \text{(II. 1)}$$

where the momenta q_i are defined in figure 1. When the total energy becomes exceedingly large a different set of variables may be convenient. These variables are natural for the simultaneous asymptotic expansion of the production amplitude in two independent subenergies,

---

*Here, and throughout this work, we use the metric $q^2 = q_0^2 - \vec{q}^2$. s, s_{12}, s_{23} are timelike (positive). t_{12}, t_{23} are usually spacelike (negative).

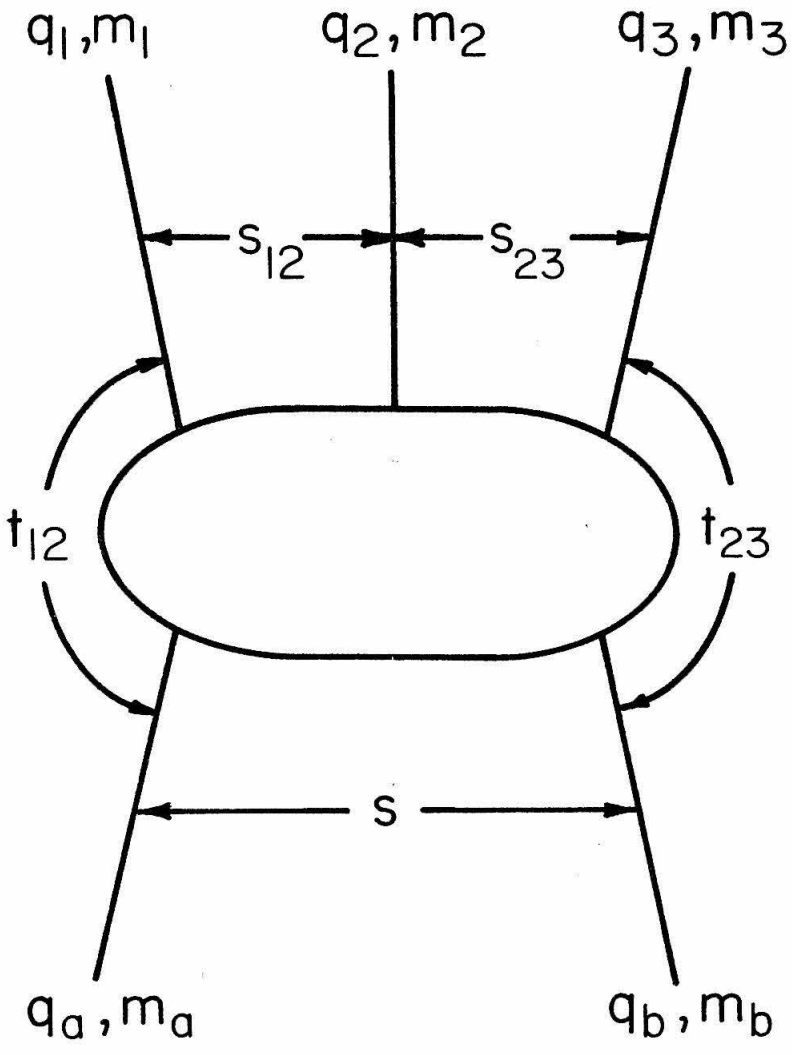

Figure 1. Particle masses, four momenta, and variables for three body final states.

corresponding to the assumption of multi-Regge dynamics. These are the Toller variables whose properties we treat in appendix A. In the three-body case, the Toller variables are t_{12}, t_{23}, $\mathrm{COSH}\xi_{12}$, $\mathrm{COSH}\xi_{23}$, and ω where

$$s_{12} = m_1^2 + m_2^2 - \frac{(t_{12} + m_1^2 - m_a^2)(t_{12} + m_2^2 - t_{23})}{2t_{12}}$$

$$- \frac{\sqrt{\lambda}(t_{12}, m_1^2, m_a^2)\,\lambda(t_{12}, m_2^2, t_{23})}{2t_{12}} \mathrm{COSH}\xi_{12}$$

$$s_{23} = m_3^2 + m_2^2 - \frac{(t_{23} + m_3^2 - m_b^2)(t_{23} + m_2^2 - t_{12})}{2t_{23}}$$

$$- \frac{\sqrt{\lambda}(t_{23}, m_3^2, m_b^2)\,\lambda(t_{12}, t_{23}, m_2^2)}{2t_{23}} \mathrm{COSH}\xi_{23}$$

$$\lambda(x, y, z) = x^2 + y^2 + z^2 - 2(xy + xz + yz) \qquad \text{(II. 2)}$$

and ω is the angle between normals defined by $\vec{q}_a \times \vec{q}_1$ and $\vec{q}_b \times \vec{q}_3$ in the frame where $\vec{q}_2 = 0$. An attractive feature is that the ranges of the new variables are independent: $1 \leq \mathrm{COSH}\xi_{12} < \infty$, $1 \leq \mathrm{COSH}\xi_{23} < \infty$, $0 \leq \omega \leq 2\pi$.

These two sets of variables share the momentum exchange variables, and for large cross channel cosines, s_{12} and s_{23} are proportional to $\mathrm{COSH}\xi_{12}$ and $\mathrm{COSH}\xi_{23}$ respectively. Their main

difference lies in the fifth variable. Since experiments are, of course, done at fixed s, the Toller variables are subject to the constraint this imposes. Consequently, the independence of the ranges of $\mathrm{COSH}\xi_{12}$, $\mathrm{COSH}\xi_{23}$, and ω is only apparent. They must vary in such a way that overall s remains constant. Theoretically, ω is a natural variable since we believe the amplitude passes to the multi-Regge form when s_{12}, s_{23} become large while ω, t_{12}, t_{23} remain fixed.

Much analysis of the multi-particle final states involves displays, or plots of the cross section partially differential in one or two of the variables employed. Phase space considerations predict a background dependence on the variables of the plot, and establish the plot boundaries. It is, however, precisely deviation from this background dependence that gives information about the dynamics. For example, enhancements in the Dalitz plot many times indicate resonances, while those in the Chew-Low plot have helped establish the presence of peripheral production mechanisms. Therefore, it is important to determine this background dependence from phase space calculations. The Lorentz invariant phase space is

$$\rho_3 = d^4q_1\, d^4q_2\, d^4q_3\, \delta(q_1^2 - m_1^2)\, \theta(q_{10})\, \delta(q_2^2 - m_2^2)\, \theta(q_{20})\, \delta(q_3^2 - m_3^2)$$

$$\times\ \theta(q_{30})\, \delta^4(q_1 + q_2 + q_3 - q_a - q_b)$$

$$= \frac{d^3q_1}{2E_1}\ \frac{d^3q_2}{2E_2}\ \frac{d^3q_3}{2E_3}\ \delta^4(q_1 + q_2 + q_3 - q_a - q_b)\,. \qquad \text{(II. 3)}$$

The background dependence comes from integrating out all variables except those of the plot. The boundaries result from keeping all quantities of ρ_3 physical.

A. The Dalitz Plot

The Dalitz plot is a display of the cross section $d^2\sigma/ds_{12}ds_{23}$ as a function of s_{12}, s_{23}, and s. In the center of mass ($\vec{q}_a + \vec{q}_b = \vec{q}_1 + \vec{q}_2 + \vec{q}_3 = 0$) we have,

$$s_{12} = (\sqrt{s} - E_3) - q_3^2 = s - 2\sqrt{s}\,E_3 + m_3^2$$

$$s_{23} = (\sqrt{s} - E_1)^2 - q_1^2 = s - 2\sqrt{s}\,E_1 + m_1^2 \quad . \qquad \text{(II. 4)}$$

So, E_1, E_3 are linearly related to s_{23}, s_{12} respectively. Phase space becomes,

$$\rho_3 = q_1 dE_1 q_3 dE_3 d\Omega_1 d\Omega_3 \frac{1}{8E_2}\,\delta(E_1+E_3-\sqrt{s}+[q_1^2+q_3^2+2\vec{q}_1\cdot\vec{q}_3+m_2^2]^{1/2})$$

$$= \frac{\pi^2}{4s}\,ds_{12}\,ds_{23}\,\theta(1 - |\hat{q}_1\cdot\hat{q}_3|) \qquad \text{(II. 5)}$$

where the theta function insures that phase space vanishes if the angle between $\vec{q}_1$ and $\vec{q}_3$ is not physical. This theta function defines the boundary of the Dalitz plot. Expressing its argument in terms of the invariants yields,

$$q_1^2 q_3^2 - (\vec{q}_1 \cdot \vec{q}_3)^2 = -\frac{1}{4s} G(s_{12}, s_{23}; s, m_2^2; m_1^2, m_3^2) \geq 0$$

(II. 6)

where the boundary is defined by the vanishing of the G function. This function is treated in some detail in Appendix B.*

Equation (II. 5) illustrates the well known fact that $\rho_3(s_{12}, s_{23})$ is independent of s_{12} and s_{23}. Hence, any non-uniformities in the plot reflect matrix element structure, and are related to the dynamics of the process. A representative Dalitz plot is shown in figure 2. Some explanation of the lines forming the central triangle is needed. In two body interactions, there is no precise way of defining the transition region between resonance behavior and smooth asymptotic variation in the overall energy. This is reflected in the uncertainty in N, the upper limit cut-off in the Finite Energy Sum Rules[7], and it hinders checking their validity. In channels where no resonances are seen, the problem does not exist, and it may be that the asymptotic or Regge amplitude continued to low energy governs the dynamics[8]. Similarly, the lines forming the central triangle of figure 2 are not precisely defined, because of uncertainties in locating the transition between resonance and asymptotic regions of s_{12}, s_{23}, and $s_{13} = (q_1 + q_3)^2$. In the following, statements referring to the "resonance" region will be subject to the ambiguities mentioned above. Region I of figure 2 will be populated when s_{12} is small and in the resonance region, so its events will come when final

---

*$G(m_d^2, m_a^2; t, s; m_c^2, m_b^2) = \varphi(s,t)$ where $\varphi(s,t) = 0$ defines the boundary of the physical region for a two-body process with the s channel being $a + b \rightarrow c + d$. See reference (6).

particles 1 and 2 are resonating. If no resonances are seen in this channel, it may be populated by events from Regge dynamics continued to low s_{12}. Actually, if duality is correct, an, as yet ill-defined, average of events in region I may be related to Regge dynamics continued to this region. Analogous statements hold for regions II and III. Overall s for this Dalitz plot is large enough so that s_{12} and s_{23} can simultaneously be out of the resonance region. When this happens we might expect the dynamics to be governed primarily by multi-Regge processes. This point will be discussed in detail in Chapter III of this work. Suffice it here to say that region IV with s_{12} and s_{23} simultaneously large may be populated by multi-Regge events with t_{12} and t_{23} simultaneously small.* Region V may be populated by multi-Regge events with large s_{23} and s_{13}, small t_{12} and $t = (q_2 - q_b)^2$. Similarly, Region VI contributions may come from multi-Regge events with large s_{12} and s_{13}, small t_{23} and $t = (q_2 - q_a)^2$. In region VII, both s_{12} and s_{23} are so large that at least one of the momentum exchanges must be large. Since no known dynamical mechanism is responsible for such events, we would expect the region to be sparsely populated which seems to be the case empirically.

---

*Events in which s_{12} and s_{23} are large with $t' = (q_1-q_b)^2$, $t'' = (q_3-q_a)^2$ both small may also populate this region. In a given reaction, however, both pairs t', t'' and t_{12}, t_{23} cannot kinematically be simultaneously small. By relabelling final particles 1 and 2 we can always choose t_{12}, t_{23} small. Analogous statements hold in the treatment of regions V and VI.

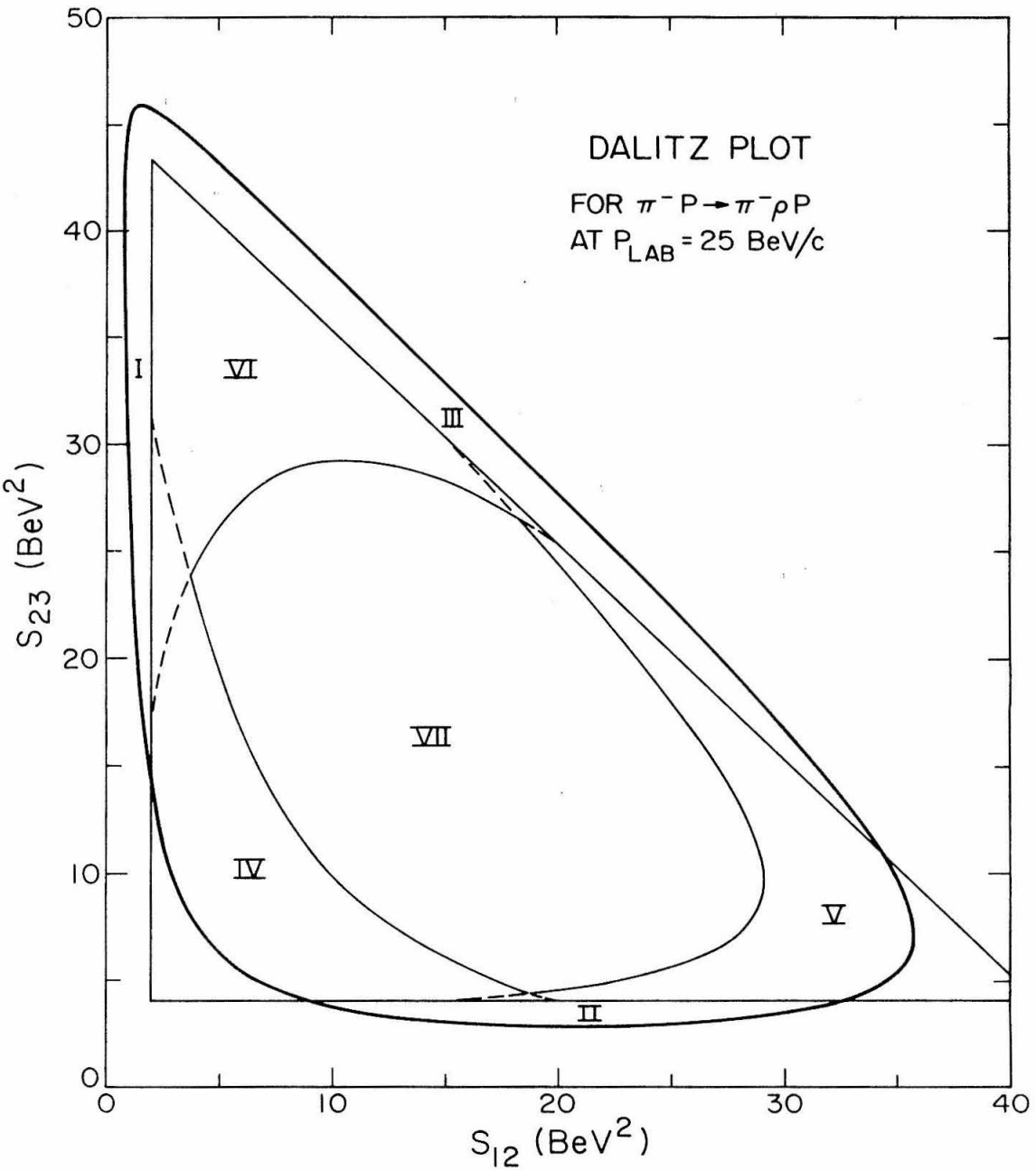

Figure 2. Dalitz Plot. The triangle is formed from the lines $s_{12} = s_{\pi\rho} = 2$ BeV^2, $s_{23} = s_{\rho p} = 4$ BeV^2, $s_{13} = s_{\pi p} = 4$ BeV^2. The lines enclosing region VII approximately correspond to the hyperbolae $s_{12}s_{23} \approx s_{12}s_{13} \approx s_{13}s_{23} \approx 100$ BeV^4.

B. The Chew-Low Plot

The Chew-Low plot is a display of the cross section $d^2\sigma/ds_{12}\, dt_{23}$ as a function of s, s_{12}, t_{23}. Other Chew-Low plots correspond to a relabelling of the particles. To compute the phase space distribution, we exploit Lorentz invariance. In the $\vec{q}_b = 0$ frame, the invariant $d^4q_3\, \delta(q_3^2 - m_3^2)\, \theta(q_{30})$ becomes

$$\frac{d^3q_3}{2E_3} = \frac{\pi}{2\sqrt{\lambda}(s,\, m_a^2,\, m_b^2)}\, ds_{12}\, dt_{23}\, \theta(1 - |\hat{q}_a \cdot \hat{q}_3|)\,. \qquad \text{(II. 7)}$$

The remainder of phase space can be treated as a two-body phase space evaluated in the $\vec{q}_1 + \vec{q}_2 = 0$ frame

$$\frac{d^2q_1}{2E_1}\,\frac{d^2q_2}{2E_2}\,\delta^4(q_1 + q_2 + q_3 - q_a - q_b) = \frac{\sqrt{\lambda}(s_{12}, m_1^2, m_2^2)}{8\, s_{12}}\, d\Omega_2. \qquad \text{(II. 8)}$$

Combining equations (II. 7) and (II. 8) we have for the complete phase space

$$\rho_3 = \frac{\pi^2}{4s_{12}}\left\{\frac{\lambda(s_{12},\, m_1^2,\, m_2^2)}{\lambda(s,\, m_a^2,\, m_b^2)}\right\}^{1/2} ds_{12}\, dt_{23}\, \theta(1 - |\hat{q}_a \cdot \hat{q}_3|) \qquad \text{(II. 9)}$$

subject to the constraint imposed by the theta function

$$q_a^2 q_3^2 - (\vec{q}_a \cdot \vec{q}_3)^2 = -\frac{1}{4m_b^2} G(t_{23}, s; s_{12}, m_b^2; m_3^2, m_a^2) \geq 0 \qquad \text{(II. 10)}$$

and the subsidiary condition that s_{12} remain physical

$$s_{12} \geq (m_1 + m_2)^2 \ . \qquad \text{(II. 11)}$$

The Chew-Low plot phase space is independent of t_{23}. Figure 3 shows a representative Chew-Low plot. The events in region I come from peripherally produced resonances decaying into final particles 1 and 2. Events in region II have s_{12} large and t_{23} small, so many of these may come from multi-Regge reactions. Events in region III have large t_{23}. When t_{23} is large, it is likely some other momentum transfer is small, so the above mentioned mechanisms corresponding to a different particle grouping could contribute to region III. In this case, we would not expect the same clustering of region III events as we see in regions I and II.

C. The t_{12} - t_{23} Plot

We have found the display of $d^2\sigma/dt_{12}\, dt_{23}$ as a function of s, t_{12}, t_{23} to be quite useful in searching for possible multi-Regge events. The multi-Regge hypothesis requires a rather severe suppression of events with either momentum transfer large, so the t_{12} - t_{23} plot provides immediate identification of multi-Regge event candidates.

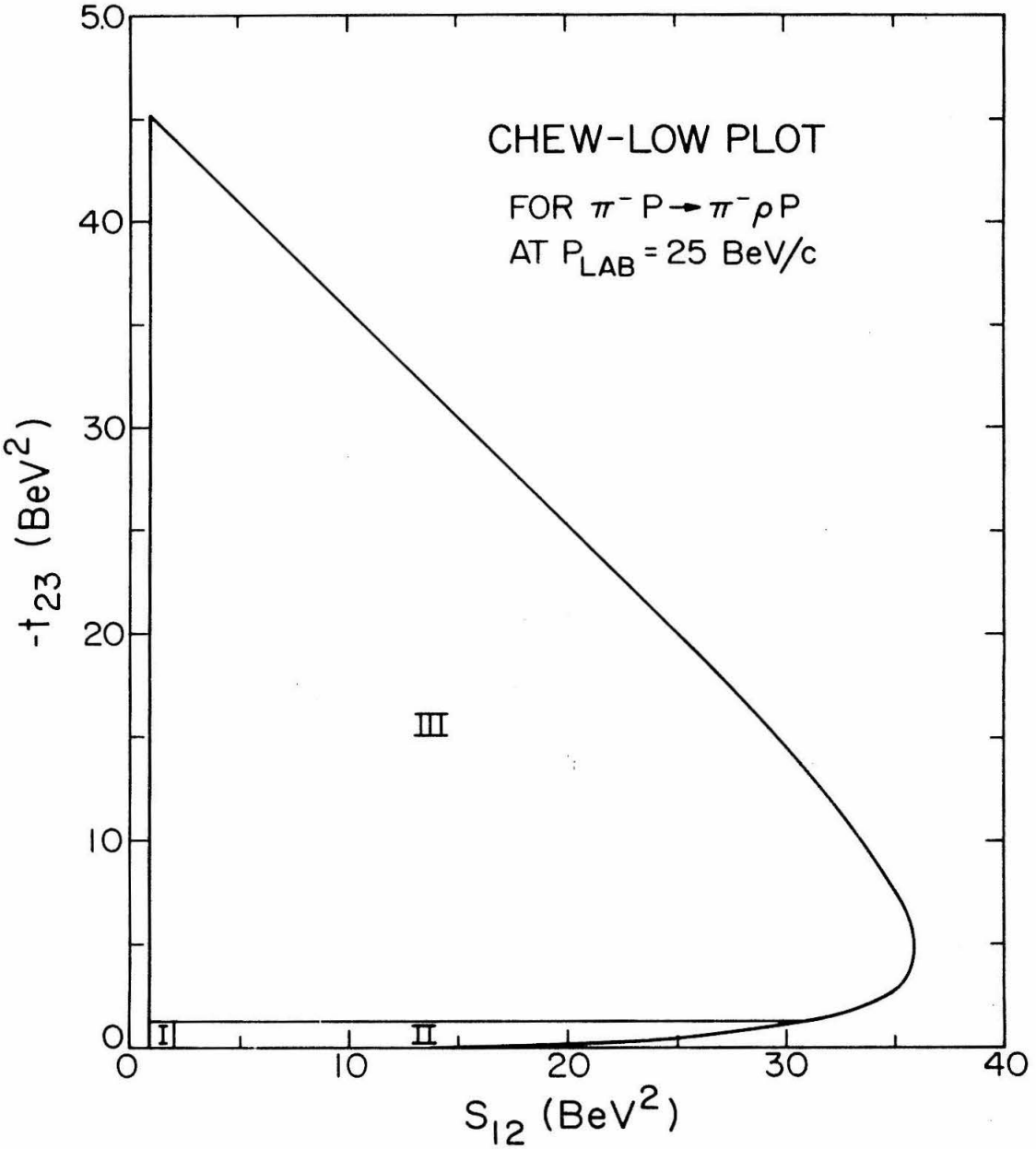

Figure 3. Chew-Low Plot. The lines $t_{23} = t_{pp} = -1$ BeV^2, $s_{12} = s_{\pi\rho} = 2$ BeV^2 divide the regions.

More care is required in obtaining the boundary to the $t_{12} - t_{23}$ plot than was necessary in the Dalitz or Chew-Low plot cases. Phase space in the center of mass frame can be written

$$\rho_3 = q_1 dE_1\, q_3 dE_3\, d\Omega_1\, d\Omega_3 \frac{1}{8E_2}\, \delta(E_1+E_3-\sqrt{s}+[q_1^2+q_3^2+2\vec{q}_1\cdot\vec{q}_3+m_2^2]^{1/2})$$

$$= \frac{\pi}{2}\, dE_1\, dE_3\, dx\, dy\, \frac{\theta(1 - x^2 - y^2 - z^2 + 2xyz)}{\sqrt{1 - x^2 - y^2 - z^2 + 2xyz}} \qquad \text{(II. 12)}$$

where $x = \hat{q}_1 \cdot \hat{q}_a$, $y = \hat{q}_3 \cdot \hat{q}_a$, and $z = \hat{q}_1 \cdot \hat{q}_3$. If we now express phase space in terms of the invariants, we find

$$\rho_3 = \frac{\pi}{16\sqrt{\lambda(s,\, m_a^2,\, m_b^2)}}\, \frac{dt_{12}\, dt_{23}\, ds_{12}\, ds_{23}\, \theta(-\Delta_4)}{\sqrt{-\Delta_4}} \qquad \text{(II. 13)}$$

where $\sqrt{s}\, q_a q_1 q_3 \sqrt{1 - x^2 - y^2 - z^2 + 2xyz} = \sqrt{-\Delta_4}$. The properties of Δ_4 have been treated thoroughly in reference (9) and in reference (10) its form is expressed explicitly in terms of the invariants. For our purposes here, we note that Δ_4 is quadratic in any of the variables s_{12}, s_{23}, t_{12}, and t_{23}, and that

$$16\,\Delta_4 = C\, s_{23}^2 + B\, s_{23} + A \qquad \text{(II. 14)}$$

where $C = \lambda(s_{12},\, t_{23},\, m_a^2) > 0$, and A, B are more complicated functions of their variables. We can perform the s_{23} integration to obtain

$$\rho_3 = \frac{\pi^2}{4\sqrt{\lambda}(s,\ m_a^2,\ m_b^2)} \frac{dt_{12}\, dt_{23}\, ds_{12}}{\sqrt{\lambda}(s_{12},\ t_{23},\ m_a^2)} \theta(B^2 - 4AC) . \qquad \text{(II. 15)}$$

A straightforward, though tedious algebraic calculation reveals that

$$B^2 - 4AC = 16\, G(t_{23},\ s;\ s_{12},\ m_b^2;\ m_3^2,\ m_a^2)$$
$$\times\ G(t_{23},\ m_1^2;\ s_{12},\ t_{12};\ m_2^2,\ m_a^2) . \qquad \text{(II. 16)}$$

Notice that the G function involving only t_{23} is that one which determines the boundary of the t_{23} - s_{12} Chew-Low plot, and hence must be negative throughout the physical region. The other G function must also be negative in the physical region to satisfy the condition prescribed by the theta function. When certain inequalities between the masses are satisfied either or both of the momentum transfers can become positive. These conditions, and the resulting t_{12} - t_{23} plot boundary will be discussed in appendix B. Here, though, we will derive the t_{12} - t_{23} boundary when the momentum transfers are always negative. Each G function is quadratic in s_{12}, so the discriminant B^2 - 4AC can be expressed as

$$B^2 - 4AC = 16 m_b^2\, t_{12}\, [s_{12} - a_+(t_{23})][s_{12} - a_-(t_{23})]$$
$$\times\ [s_{12} - b_+(t_{12},\ t_{23})]\ [s_{12} - b_-(t_{12},\ t_{23})] \qquad \text{(II. 17)}$$

where

$$a_{\pm}(t_{23}) = s + m_3^2 - \frac{(m_b^2 + s - m_a^2)(m_b^2 + m_3^2 - t_{23})}{2m_b^2}$$

$$\pm \frac{\sqrt{\lambda}(s, m_b^2, m_a^2)\,\lambda(m_b^2, m_3^2, t_{23})}{2m_b^2}$$

$$b_{\pm}(t_{12}, t_{23}) = m_1^2 + m_2^2 - \frac{(t_{12} + m_2^2 - t_{23})(t_{12} + m_1^2 - m_b^2)}{2t_{12}}$$

$$\pm \frac{\sqrt{\lambda}(t_{12}, t_{23}, m_2^2)\,\lambda(t_{12}, m_1^2, m_b^2)}{2t_{12}}. \quad \text{(II. 18)}$$

With the condition that $t_{12}, t_{23} < 0$, s_{12} is always greater than $a_-(t_{23})$ and $b_+(t_{12}, t_{23})$. Hence the physical region occurs for $b_-(t_{12}, t_{23}) \leq s_{12} \leq a_+(t_{23})$. Performing the s_{12} integration between these limits gives

$$\rho_3 = \frac{\pi^2}{2\sqrt{\lambda}(s, m_a^2, m_b^2)} dt_{12} dt_{23} \left\{ \ell n \left| \frac{4t_{12}t_{23}(s - m_a^2 - m_b^2 + \sqrt{\lambda}(s, m_a^2, m_b^2))}{m_2^2 - t_{23} - t_{12} + \sqrt{\lambda}(t_{12}, t_{23}, m_2^2)} \right| \right.$$

$$- \ell n \left| (m_3^2 - m_b^2 - t_{23} + \sqrt{\lambda}(m_3^2, m_b^2, t_{23}))(m_1^2 - m_a^2 - t_{12} \right.$$

$$\left. \left. + \sqrt{\lambda}(m_1^2, m_a^2, t_{12})) \right| \right\}. \quad \text{(II. 19)}$$

From this expression we see that, while phase space is not independent of t_{12} and t_{23}, its variation with them is only logarithmic. Phase space vanishes at the boundary which is defined by the condition $a_+(t_{23}) = b_-(t_{12}, t_{23})$. Figures 4 and 5 illustrate the t_{12} - t_{23} plot. In 4 we see a phase space contour plot for an area in which both t_{12} and t_{23} are simultaneously small. Multi-Regge events may contribute strongly to such an area. In fact, a density of events considerably greater than that of phase space is a necessary condition if the multi-Regge hypothesis is to be tenable. For most practical purposes, the corner boundary where both t's are small may be treated as a sharply rectangular corner. Figure 5 illustrates the complete t_{12} - t_{23} plot with the rectangle at the origin indicating the region where the multi-Regge event contribution should be largest.

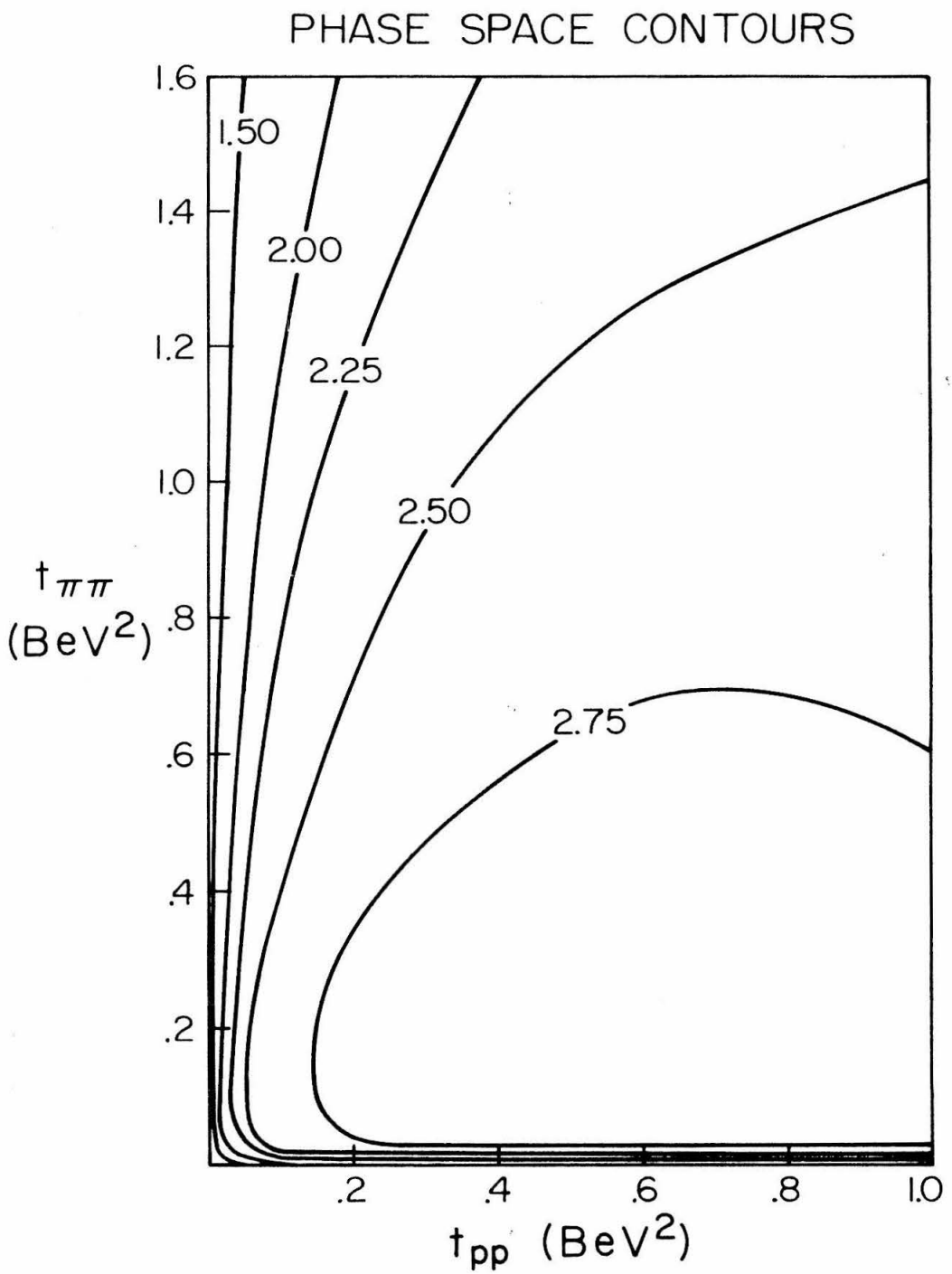

Figure 4. Contour plot exhibiting slow phase space variation except at plot boundaries where it vanishes. Phase space is for the reaction $\pi^- p \rightarrow \pi^- \rho p$ at P_{LAB} = 25 BeV/c.

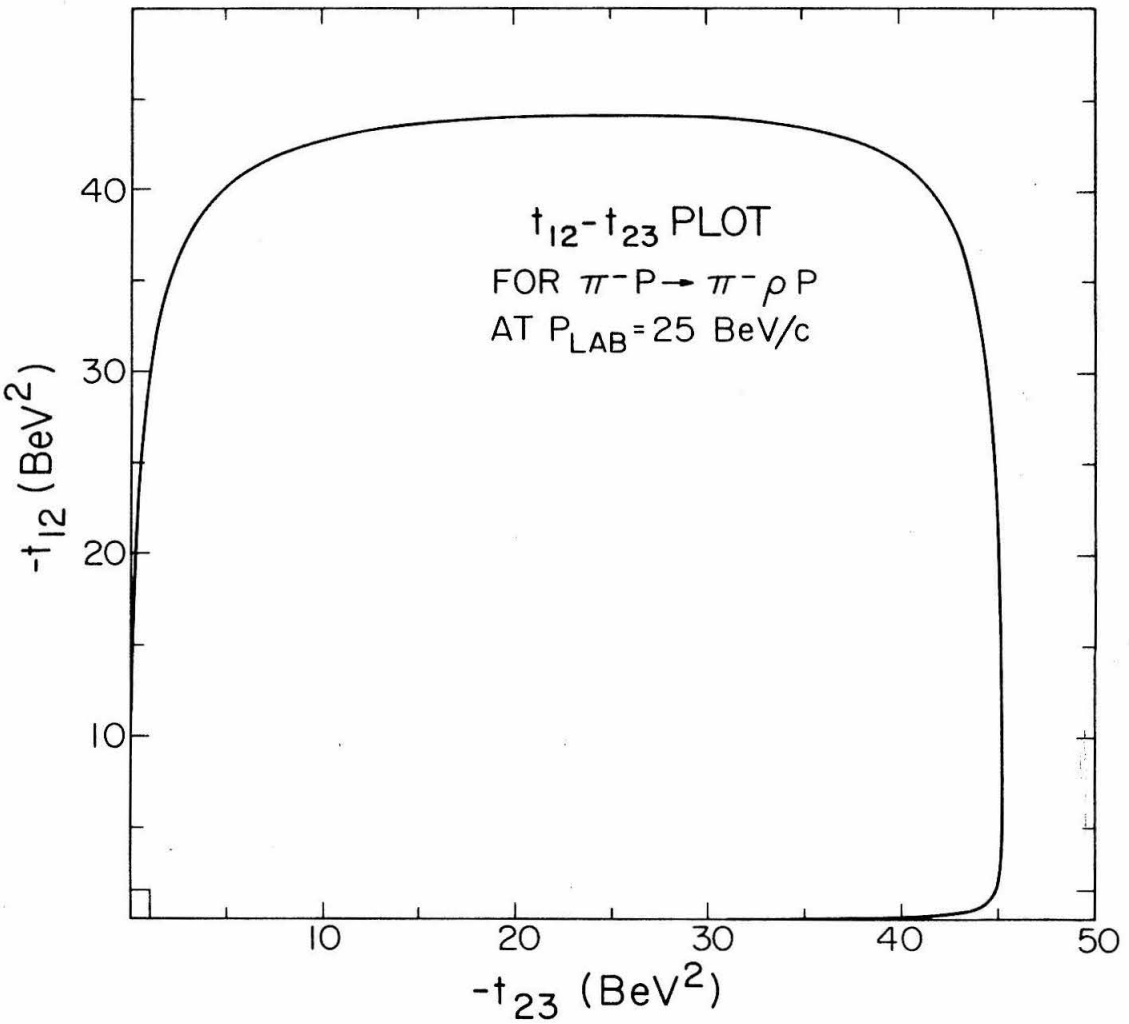

Figure 5. t_{12} - t_{23} Plot. The lines $t_{12} = t_{\pi\pi} = -1.6$ BeV^2, $t_{23} = t_{pp} = -1$ BeV^2 give the region of the figure (4) plot.

CHAPTER III

Multi-Regge Dynamics

A. Multi-Regge Hypothesis

It has been conjectured independently by several authors[3, 4, 5] that the multi-particle production amplitude, in a certain well-defined kinematic region, is essentially the product of two body Regge amplitudes. For analyses involving differential cross sections in which the spin of all external particles is summed over, these treatments provide an accurate statement of the MRE hypothesis; we simply interpret the Regge residues derived for spinless scattering as spin-averaged residues. For the sake of simplicity and because the analysis of Chapter IV involves spin-averaged cross sections, for the present we will restrict ourselves to high energy scattering of spinless particles. The complications due to spin are treated in appendix C.

We consider the process (see figure 6)

$$a + b \rightarrow 1 + \cdots + N \qquad \text{(III. 1)}$$

and, initially, deal with the special case $N = 3$. In accord with the two body Regge assumptions, at high energies we might expect the amplitude of channel (III. 1) (hereafter referred to as the direct channel) to be dominated by Regge exchange in the cross channel

$$a + \bar{1} \rightarrow \bar{b} + 2 + 3 . \qquad \text{(III. 2)}$$

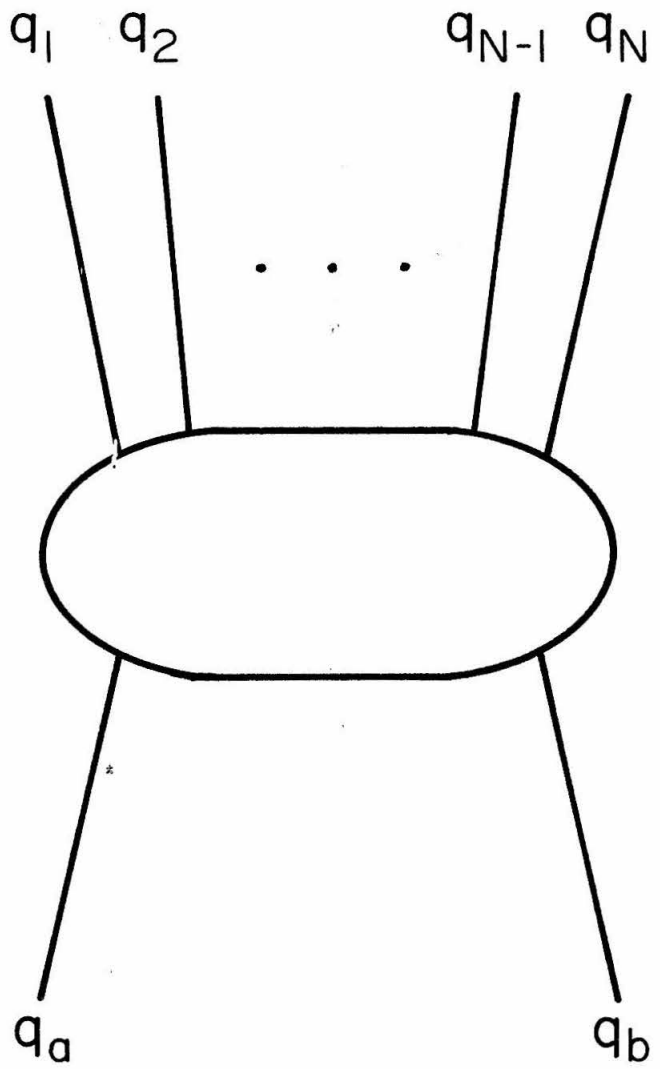

Figure 6. Particle four momenta for the reaction a+b → 1+...+N.

In the center of mass of 3, $\bar{b}$ ($\vec{q}_3 + \vec{q}_{\bar{b}} = 0$), we couple $\bar{b}$ and 3, transform to the center of mass of a, $\bar{1}$, and couple to particle 2. The amplitude for the initial state to scatter into this state can, after a partial wave expansion, be expressed as[3]

$$A(s,t_{12},t_{23},\theta_{12},\theta_{23},\varphi) = \sum_{j_1,j_2,\lambda} A_{j_1 j_2 \lambda}(s,t_{12},t_{23})\, e^{i\lambda\varphi} \times d^{j_1}_{\lambda 0}(-\theta_{12})\, d^{j_2}_{0\lambda}(-\theta_{23}) \qquad \text{(III. 3)}$$

where θ_{12} is the angle between $\vec{q}_{\bar{1}}$ and $\vec{q}_2$ in the frame $\vec{q}_a + \vec{q}_{\bar{1}} = 0$, θ_{23} is the angle between $\vec{q}_2$ and $\vec{q}_3$ in the frame $\vec{q}_{\bar{b}} + \vec{q}_3 = 0$, and φ is the angle between $\vec{q}_{\bar{1}} \times \vec{q}_a$ and $\vec{q}_{\bar{b}} \times \vec{q}_3$ in the rest frame of particle 2. We now assume $A_{j_1 j_2 \lambda}(s,t_{12},t_{23})$ is a meromorphic function in the right-half j_1 and j_2 planes possessing the same singularities at $j_1 = \alpha_1(t_{12})$, $j_2 = \alpha_2(t_{23})$ that would be allowed in the corresponding channels for two body processes. We then perform a double Sommerfeld-Watson transformation, and analytically continue the amplitude to the direct channel. In this continuation, $\cos\theta_{12}$ and $\cos\theta_{23}$ become the $\cosh\xi_{12}$ and $\cosh\xi_{23}$ of Eq. (II. 2), and, hence, are proportional to s_{12} and s_{23} respectively when these subenergies become large. The continuation of the angle φ is the angle ω (see reference (11)) discussed in Chapter II. We now assume $A_{j_1 j_2 \lambda}(s,t_{12},t_{23})$ factorizes as in two body Reggeism, so that as $\cosh\xi_{12}$, $\cosh\xi_{23}$ (and hence also s_{12}, s_{23}) simultaneously become large while t_{12}, t_{23}, and ω are held fixed, the

amplitude receives contributions of the form

$$A(s,t_{12},t_{23},s_{12},s_{23}) \underset{s_{12},s_{23}\to\infty}{\sim} \beta_{a\alpha_1 1}(t_{12})\, s_{12}^{\alpha_1(t_{12})}\, \zeta_1(t_{12})$$

$$\times \gamma_{\alpha_1 2\,\alpha_2}(t_{12},\omega,t_{23})\, s_{23}^{\alpha_2(t_{23})}\, \zeta_2(t_{23})\, \beta_{b\alpha_2 3}(t_{23})$$

$$\zeta_k(t) = \frac{1 \pm \exp(-i\pi\alpha_k(t))}{\Gamma[1+\alpha_k(t)]\cdot \mathrm{SIN}\,\pi\alpha_k(t)}\ ,\ k=1,2 \qquad \text{(III. 4)}$$

where the residues $\beta_{a\alpha_1 1}(t_{12})$, $\beta_{b\alpha_2 3}(t_{23})$ are usual two body Regge residues for the corresponding vertices and $\gamma_{\alpha_1 2\alpha_2}(t_{12},\omega,t_{23})$ is the middle vertex Regge residue resulting from the sum over λ in Eq. (III. 3).

A generalization of this procedure can be applied to obtain the N body multi-Regge amplitude. In the cross channel

$$a + \bar{1} \quad \bar{b} + 2 + \cdots + N \qquad \text{(III. 5)}$$

we couple particles N and $\bar{b}$ in their center of mass, transform to the center of mass of particles N - 1, N, and $\bar{b}$ and couple to N - 1, and repeat this procedure until we transform to the center of mass of a, $\bar{1}$, and couple to 2 to form the final state, we then make a partial wave expansion of the amplitude that this final state was reached from the initial state. We assume this resulting

amplitude is meromorphic in the right-half $j_1, \ldots, j_{N-1}$ planes, so after a multiple Sommerfeld-Watson transformation, the amplitude can be analytically continued to the direct channel. The continuation of the variables analogous to $\cos\theta_{12}$, $\cos\theta_{23}$, and φ in the three body case are the Toller variables $\cosh\xi_{i,i+1}$ ($i = 1, \ldots, N-1$) and ω_i ($i = 2, \ldots, N-1$) discussed in appendix A. Assuming factorization at each vertex, we see that as these $\cosh\xi_{i,i+1}$ (and the corresponding subenergies $s_{i,i+1}$) become large while the momentum exchanges $t_{i,i+1}$ and angles ω_i are held fixed, the multi-Regge form for the amplitude is obtained:

$$A(s_{i,i+1}, t_{i,i+1}, \omega_i) s_{12}, s_{23}, \ldots, s_{N-1,N} \to \infty \sim \beta_{a\alpha_1 1}(t_{12}) s_{12}^{\alpha_1(t_{12})} \zeta_1(t_{12})$$

$$\times \gamma_{\alpha_1 2 \alpha_2}(t_{12}, \omega_2, t_{23}) \cdots s_{N-1,N}^{\alpha_{N-1}(t_{N-1,N})} \zeta_{N-1}(t_{N-1,N}) \beta_{b\alpha_{N-1}N}(t_{N-1,N})$$

$$\zeta_k(t) = \frac{1 \pm \exp(-i\pi\alpha_k(t))}{\Gamma(1+\alpha_k(t)) \sin\pi\alpha_k(t)}, \quad k = 1, \ldots, N \qquad \text{(III. 6)}$$

where trajectory $\alpha_1(t_{12})$ couples to a and 1 with strength $\beta_{a\alpha_1 1}(t_{12})$, trajectories $\alpha_1(t_{12})$ and $\alpha_2(t_{23})$ couple to 2 through residue $\gamma_{\alpha_1 2 \alpha_2}(t_{12}, \omega_2, t_{23})$; etc. until trajectory $\alpha_{N-1}(t_{N-1,N})$ couples to b and N with strength $\beta_{b\alpha_{N-1}N}(t_{N-1,N})$.

It is inherent in the MRE hypothesis that the trajectories $\alpha_i(t_{i,i+1})$ of Eq. (III. 6) are determined only by the quantum numbers of the allowed exchanges between clusters i and i+1. This means that these trajectories are identical to the familiar two body

trajectories about which something is known. Therefore, any check of the MRE hypothesis must show a definite correspondence between the trajectories of the reaction and the known two body trajectories. Even in principle, however, demonstration of this correspondence is not as unambiguous as we might hope. The coupling of two "Reggeons" to a single external particle or cluster is unknown. Nevertheless, theoretical investigation of this coupling can be performed. For example, we can use a model for Regge behavior originally proposed by Durand, Feynman, and Van Hove[12] and developed by Blankenbecler, Sugar, and Sullivan[13]. We specialize to the case of three body final states, where the bi-Reggeon coupling first appears, being a function of t_{12}, t_{23}, and ω. Within the framework of the model, there always exist couplings that require no ω dependence. When present, the ω dependence in the high energy limit comes from the variable $s/s_{12}s_{23}$, where

$$s \underset{s_{12},s_{23}\to\infty}{\sim} \frac{s_{12}\,s_{23}}{\lambda(t_{12},t_{23},m_2^2)}\left[m_2^2-t_{12}-t_{23}+2\sqrt{-t_{12}}\sqrt{-t_{23}}\cos\omega\right]. \qquad \text{(III. 7)}$$

Since experiments are performed at fixed s, the ω dependence changes the powers of s_{12}, s_{23} in the amplitude, and, hence, the effective trajectory intercepts. By considering the cross section variation in the subenergies, we can determine if ω dependence is required. In the particular reaction we consider in Chapter IV, no ω dependence is necessary, a result consistent with the trajectory intercepts having their two body values.

Since the choice of contributing trajectories depends entirely on the quantum numbers allowed in the exchange, the considerations

necessary for making this choice are the same as in two body interactions. For isospin zero, dominant contributions should come from Pomeranchon and P' exchanges for positive G-parity, and from ω exchange for negative G-parity. For isospin one, dominant contributions should come from ρ exchange for positive G-parity and from π and A_2 exchange for negative G-parity. The complexities associated with π exchange[14] in two body interactions, along with the relative simplicity of ρ and possibly A_2 exchange, should carry over to multi-Regge processes. The P' and π contributions should decrease relative to those of the Pomeranchon and A_2 respectively as the energy increases. For baryon exchanges, the nucleon and N*(1238) should dominate their respective isospin channels. For non-zero strangeness exchanges similar consideration apply.

B. Cuts in the Data

To investigate the multi-Regge hypothesis, it is necessary to impose certain restrictions on the data to be analyzed. Five main considerations require these cuts in the data.

First, when identical particles appear in the final state, we cannot, in general, determine which one came from a specified cluster. Consequently, we cannot overcome the inherent ambiguity of grouping the final particles into the clusters of the reaction. We do, nevertheless, avoid these difficulties to a large extent by analyzing the grouping that allows the smallest momentum transfers to be reached. This rule is consistent with the spirit of multiperipheralism. While this procedure does not eliminate classes of events as cuts in the data do, it does eliminate certain groupings. For this reason, we list it as one of the types of restrictions to be imposed on the data.

Second, multi-Regge events should contribute to processes in which all systems of two adjacent clusters have large invariant masses and all momentum transfers connecting adjacent clusters are small. Thus, the kinematic regions receiving contributions from multi-Regge processes are well-defined except for the ambiguities discussed in Chapter II concerning the transition region between resonance and asymptotic energies. To insure that the requirements of the hypothesis are met, the only events kept are those having all invariant masses, or subenergies, of two adjacent clusters in the asymptotic region. It should be noted, however, that if we believe we understand duality we may want to continue the multi-Regge amplitude to low subenergies. Other workers have performed their analyses in this kinematic region[15]. We should emphasize that this practice introduces additional theoretical assumptions, and, therefore, is not as clean a test of multi-Reggeism.

Third, according to the hypothesis, when the invariant mass of a cluster reaches the asymptotic region, the cluster breaks up into two clusters connected by a Regge exchange. For simplicity, we wish to avoid analyzing events that may be described by multi-Regge amplitudes corresponding to different numbers of Regge exchanges. Therefore, in any one investigation, we fix the number of Regge exchanges, and discard all events in which any clusters in the process have invariant masses in the asymptotic region. Duality, of course, does not allow the one to one correspondence between Regge exchange and asymptotic subenergies of adjacent clusters; if it is employed, this cut in the data does not apply.

Fourth, for most subenergies encountered in practice, particles from different clusters can resonate, leading to final state interactions that can complicate the multi-Regge amplitude.

To avoid these complications, we eliminate all events in which any invariant mass of particles from different clusters lies in the resonance band. In particular, this problem disappears with increasing subenergies, but these cuts are many times necessary at present machine energies.

Fifth, multi-Regge events must be multi-peripheral since the $(s_{i,i+1})^{\alpha_i(t_{i,i+1})}$ and residue factors of Eq. (III. 6) decrease rapidly with increasing momentum transfer $t_{i,i+1}$. It is crucial to establish the multi-peripheral nature of potential multi-Regge events since it is a necessary condition of the hypothesis. Assuming this has been established, we can proceed in two ways. First, if fits to two body Regge data for momentum transfers greater than the order of one BeV^2 are available, we can use them in Eq. (III. 6). These large t fits permit a larger data sample, and, hence, increase statistics. Second, as is more likely, if these fits do not exist, or if we have confidence only in the more accurate small t fits, we eliminate events with momentum transfer larger than that of the fits.

C. Distributions as Checks of the Multi-Regge Hypothesis

To check the multi-Regge hypothesis we must compare experimental data with theoretical distributions of the cross section differential in various combinations of the variables of the process. A process at fixed beam energy with an N body final state depends on 3N-5 variables. Considering that we can form distributions differential in 3N-5, 3N-4, . . . , 1, or 0 variables (by successive integration), we see that there are 2^{3N-5} possible distributions for each set of variables. We will discuss only a few of these types, namely

distributions differential in all variables, one variable, and no variables (where it is understood that the cross section depends on overall energy and the particle masses).

Recall that in two body reactions, analysis of the cross section differential in all variables gives the absolute value of the amplitude. Fits are made to the distribution in momentum transfer t (the 3N-5 "variables" in this case) for different beam energies. When the flux and phase space factors are divided out, the resulting function of s and t is the absolute value squared of the amplitude. In principle, an analogous procedure is possible for N body final states. We would partition phase space into bins sufficiently small so that the amplitude would be roughly constant over each bin. The experimental events would be placed in the bins, and, for a given form of the amplitude, a fit to the data would be made. In practice, no experiment to date has produced sufficient statistics to implement this approach in the kinematic region which should receive multi-Regge contributions. We discuss it here only because it seems to be a simple way to obtain the amplitude and may be of use when future experiments are performed. For any analysis at this time, we must integrate over certain variables to increase the statistics.

In our investigations, we integrate over all but one variable. In discussing these distributions, for simplicity we restrict ourselves to three body final states. Final states with more particles are no more complicated in principle, but the increased number of phase space integrations makes the analysis more tedious. The MRE amplitude for three body final states is given by Eq. (III. 4). To proceed in the analysis we must assume an explicit form for the couplings. To this end we assume:

(a) Spin dependence may be neglected; the spinless residues are "effective" spin-averaged residues.

(b) The signature factors $\zeta_k(t)$ are slowly varying in t and may be set equal to constants

(c) The trajectories are linear about $t = 0$.

(d) The end vertices may be parameterized as

$$\beta_{a\alpha_1 2}(t_{12}) \propto e^{b_1 t_{12}}, \quad \beta_{b\alpha_2 3}(t_{23}) \propto e^{b_2 t_{23}}$$

(e) The middle vertex may be parameterized by

$$\gamma_{\alpha_1 2 \alpha_2} \propto e^{g_1 t_{12} + g_2 t_{23}}, \text{ independent of } \omega .$$

Assumption (e) is the strongest of these assumptions. Since we would expect that g_1 and g_2 depend on particle 2, the assumption is that the dependence is "smooth" so that g_1, g_2 may be taken to represent average values of these exponential factors. Also, the lack of ω dependence must be closely checked for experimental consistency.

With these assumptions, the three body multi-Regge amplitude becomes

$$A = N e^{c_1 t_{12}} (s_{12}/s_0)^{\alpha_1(0) + \alpha'_1(0) t_{12}} (s_{23}/s_0)^{\alpha_2(0) + \alpha'_2(0) t_{23}}$$

$$\times e^{c_2 t_{23}}, \quad c_i = b_i + g_i, \quad i = 1, 2 \qquad \text{(III. 8)}$$

where N, having the dimension of length, is the product of the three coupling constants, and s_0 is a scaling factor. This form can be used to make predictions for all distributions. The differential

cross section for the process of Eq. (III. 1) with N=3 is given by

$$d\sigma_3 = \frac{1}{(2\pi)^5} \frac{1}{2\sqrt{\lambda}(s, m_a^2, m_b^2)} |A|^2 \rho_3 \qquad \text{(III. 9)}$$

where $\sqrt{\lambda}(s, m_a^2, m_b^2)$ is proportional to the incident flux and ρ_3 is the Lorentz invariant three body phase space.

1. s Distributions

For distributions over the subenergies s_{12}, s_{23}, the cross section is integrated over both momentum transfers. This integration is done in closed form in reference (11). We use the phase space expansion of Eq. (II. 12). The cross section becomes

$$d\sigma_3 = \frac{N^2}{(2\pi)^5} \frac{1}{2^4 \sqrt{\lambda}(s, m_a^2, m_b^2)} \left(\frac{s_{12}}{s_0}\right)^{2\alpha_1} e^{2\Omega_1(m_1^2+m_a^2-2E_1E_a)} \left(\frac{s_{23}}{s_0}\right)^{2\alpha_2}$$

$$\times e^{2\Omega_2(m_3^2 + m_b^2 - 2E_3E_b)} \frac{\pi}{s} ds_{12}\, ds_{23}\, I$$

$$\Omega_i = c_i + \alpha_i' \ln (s_{i,i+1}/s_0) \quad , \quad i = 1, 2$$

$$I = \int dx\, dy\, e^{\Gamma_1 x} e^{-\Gamma_2 y} \frac{\theta(1 - x^2 - y^2 - z^2 + 2xyz)}{[1 - x^2 - y^2 - z^2 + 2xyz]^{1/2}}$$

$$\Gamma_i = 2\Omega_i (2\, q_{2i-1}\, q_a) \quad , \quad i = 1, 2 \qquad \text{(III. 10)}$$

where E_i, q_i, $i = 1, 3, a, b$, are the center of mass energy and momentum and x, y, z are defined in Chapter II. Notice that

$$\frac{dx}{[1 - x^2 - y^2 - z^2 + 2xyz]^{1/2}} = -d[\cos^{-1}(\frac{x - yz}{\sqrt{1-z^2}\sqrt{1-y^2}})] \equiv du \qquad \text{(III. 11)}$$

so

$$I = \frac{1}{2}\int_{-1}^{1} dy\, e^{-(\Gamma_2 - \Gamma_1 z)y} \int_0^{2\pi} du\, e^{\Gamma_1(\sqrt{1-z^2}\sqrt{1-y^2})\cos u}$$

$$= \frac{1}{2}\int d\Omega_r\, e^{\vec{\Gamma}\cdot\hat{r}} = \frac{2\pi \sinh \Gamma}{\Gamma} \qquad \text{(III. 12)}$$

where $\vec{\Gamma} = (\Gamma_1\sqrt{1 - z^2}, 0, \Gamma_1 z - \Gamma_2)$, and $\Gamma = |\vec{\Gamma}| = \sqrt{\Gamma_1^2 + \Gamma_2^2 - 2\Gamma_1\Gamma_2 z}$.

Unfortunately, we cannot obtain the distribution $d\sigma/ds_{ij}$ in closed form; the remaining integral must be done by machine. The limits on this integration are the Dalitz plot boundaries subject to restriction imposed by cuts.

2. t Distribution

If we assume any cuts in the momentum transfer exclude regions which receive an insignificant contribution from the multi-Regge amplitude, then we can analytically perform one of the integrations in the t distribution.

For the phase space expression we use

$$\rho_3 = \frac{\pi}{8s} ds_{12}\, ds_{23} \frac{dt_{23}}{2q_3 q_a} dx \frac{\theta(1 - x^2 - y^2 - z^2 + 2xyz)}{\sqrt{1 - x^2 - y^2 - z^2 + 2xyz}}. \qquad \text{(III. 13)}$$

The differential cross section is

$$d\sigma_3 = dt_{23}\, ds_{12}\, ds_{23} \{ e^{2c_2 t_{23}} \left(\frac{s_{12}}{s_0}\right)^{2\alpha_1} \left(\frac{s_{23}}{s_0}\right)^{2\alpha_2(t_{23})}$$

$$\times e^{2\Omega_1(m_1^2 + m_a^2 - 2E_1E_a)} \frac{1}{\sqrt{\lambda(s, s_{12}, m_3^2)}} \} \; J\, K$$

$$J = \int_0^\pi e^{4\Omega_1 q_1 q_a (yz + \sqrt{1-y^2}\sqrt{1-z^2}\cos u)}\, du$$

$$K = \frac{1}{(2\pi)^5} \frac{\pi}{2^3} \frac{N^2}{\sqrt{\lambda(s, m_a^2, m_b^2)}} \,. \qquad \text{(III. 14)}$$

The integral J is elementary yielding

$$J = \pi\, e^{4\Omega_1 q_1 q_a yz}\, I_0(4\Omega_1 q_1 q_a \sqrt{1-y^2}\sqrt{1-z^2}) \qquad \text{(III. 15)}$$

where $I_0(x)$ is the zeroth order modified Bessel function. To obtain $d\sigma_3/dt_{23}$ we must do the remaining two integrations over s_{12} and s_{23} by machine. For fixed t_{23} and s_{12}, the range of s_{23} dictated by phase space is

$$s_{23} = A + B\,r\,, \quad -1 \le r \le 1$$

$$A = m_2^2 + m_3^2 + \frac{(s - s_{12} - m_3^2)(s_{12} + m_2^2 - m_1^2)}{2s_{12}}$$

$$B = \frac{\sqrt{\lambda}(s,\ s_{12},\ m_3^{\,2})\ \lambda(s_{12},\ m_2^{\,2},\ m_1^{\,2})}{2s_{12}} \ . \qquad \text{(III. 16)}$$

Notice that the s_{23} limits are on the Dalitz plot boundary. Their dependence on t_{23} is implicit, being determined by the Chew-Low s_{12} - t_{23} plot boundaries. Naturally, cuts in the data modify these integration limits.

Of course, an analogous procedure gives $d\sigma_3/dt_{12}$.

3. ω Distribution

The variation of the cross section with the variable ω gives information about the internal vertex at which two "Reggeons" couple to an external particle. In Chapter II we saw that ω is the angle in the rest frame of particle 2 between the normal to the plane determined by particles a and 1 and the normal to the plane determined by particles b and 3. From the Eq. (A. 11) of appendix A, we have that, in frame $(1,\ \ell)$, the momentum four vector of particle b is

$$q_b(1,\ \ell) = L(q_{12})\ L(\gamma_2)\ L(q_{23})\ q_b(2,\ r) \qquad \text{(III. 17)}$$

where $q_b(2,\ r)$ is in the standard form $(E_b,\ 0,\ 0,\ q_b)$. Thus, the overall invariant mass is

$$s = (-q_a + q_b)^2 = m_a^{\,2} + m_b^{\,2} - 2q_a(1,\ \ell) \cdot q_b(1, \ell) \ . \qquad \text{(III. 18)}$$

Carrying out the operations of Eqs. (III. 17) and (III. 18), we find

$$s = m_a^2 + m_b^2 + 2E_a E_b \{\mathrm{COSH}\xi_{12}\,\mathrm{COSH}\gamma_2\,\mathrm{COSH}\xi_{23} + \mathrm{SINH}\xi_{12}\,\mathrm{COS}\omega \times \mathrm{SINH}\xi_{23}\} + 2\mathrm{SINH}\gamma_2 \{\mathrm{COSH}\xi_{12}\, q_b E_a + \mathrm{COSH}\xi_{23}\, E_b q_a\} + 2\,\mathrm{COSH}\gamma_2\, q_a\, q_b$$

$$E_a = \frac{\sqrt{\lambda}(t_{12}, m_a^2, m_1^2)}{2\sqrt{-t_{12}}}, \quad E_b = \frac{\sqrt{\lambda}(t_{23}, m_b^2, m_3^2)}{2\sqrt{-t_{23}}},$$

$$\mathrm{COSH}\gamma_2 = \frac{m_2^2 - t_{12} - t_{23}}{2\sqrt{-t_{12}}\sqrt{-t_{23}}}. \qquad \text{(III. 19)}$$

Equation (III. 19) expresses $\mathrm{COS}\omega$ in terms of the variables of Eq. (II. 1), when we consider the linear relationship between s_{ij} and $\mathrm{COSH}\xi_{ij}$. To obtain the cross section as a function of ω, it is convenient to express phase space in the Toller variables[16]. For the three body final state phase space is

$$\rho_3 = \frac{2\pi}{2^6(-t_{12})(-t_{23})\sqrt{\lambda}(s, m_a^2, m_b^2)} \sqrt{\lambda}(t_{12}, m_1^2, m_a^2)\lambda(t_{12}, t_{23}, m_2^2)\lambda(t_{23}, m_3^2, m_b^2) \times dt_{12}\, dt_{23}\, d(\mathrm{COSH}\xi_{12})\, d(\mathrm{COSH}\xi_{23})\, d\omega\, \delta(s - s(\omega, t_{12}, t_{23}, \xi_{12}, \xi_{23})) \qquad \text{(III. 20)}$$

where $s(\omega, t_{12}, t_{23}, \xi_{12}, \xi_{23})$ is given by Eq. (III. 19). When Eq. (III. 20) is substituted into Eq. (III. 9), only the integration removing the δ-function can be performed analytically. Assume this is done with the $\mathrm{COSH}\xi_{12}$ integration. Then, the curve of Eq. (III. 19) defines the

range of the $\mathrm{COSH}\xi_{12}$ integration for fixed s, t_{12}, t_{23}, and ω. The limits of the remaining two integrations over t_{12} and t_{23} are independent of the value of ω, provided there are no cuts in s_{12} and s_{23}. They are given by the t_{12} - t_{23} plot boundary discussed in Chapter II. The points on this boundary satisfy Eq. (III. 19) with $\mathrm{COSH}\xi_{12} = \mathrm{COSH}\xi_{23} = 1$, provided t_{12} and t_{23} never become positive. When cuts are made in s_{12} and s_{23}, we must determine the corresponding limitations on $\mathrm{COSH}\xi_{12}$ and $\mathrm{COSH}\xi_{23}$, impose these restrictions on Eq. (III. 19), and solve for the t_{12} - t_{23} boundary for fixed values of ω. In practice, this procedure usually must be carried out numerically.

4. Treiman-Yang Angle

The Treiman-Yang test[17] provides a necessary condition that must be satisfied for any zero helicity exchange. This test requires that the cross section for a zero helicity exchange be invariant under rotations about the momentum direction of the exchanged object in the rest frame of one of the incident particles. If this incident particle is particle a, then the Treiman-Yang angle, in the $\vec{q}_a = 0$ frame, is defined by

$$\cos\gamma = \frac{(\vec{q}_b \times \vec{q}_3) \cdot (\vec{q}_1 \times \vec{q}_2)}{|\vec{q}_b \times \vec{q}_3| \quad |\vec{q}_1 \times \vec{q}_2|} \qquad \text{(III. 21)}$$

where $\vec{q}_1 + \vec{q}_2 = \vec{q}_b - \vec{q}_3$ is the direction of the exchanged object's momentum. The angle is invariant under Lorentz transformations in this momentum direction, so, for convenience, we boost to the frame in which $\vec{q}_1 + \vec{q}_2 = 0$. Then, we can use Eqs. (II. 7, II. 8) for the phase space

$$\rho_3 = \frac{\pi}{16\sqrt{\lambda(s, m_a^2, m_b^2)}}\, ds_{12}\, dt_{23}\, \frac{\sqrt{\lambda(s_{12}, m_1^2, m_2^2)}}{s_{12}}\, dr\, d\gamma \qquad \text{(III. 22)}$$

where the range of the angular integration is independent of s_{12} and t_{23} values: $-1 \le r \equiv \hat{q}_a \cdot \hat{q}_2 \le 1$, $0 \le \gamma \le 2\pi$. The remaining invariants can be expressed in terms of the variables s_{12}, t_{23}, r, γ as follows

$$t_{12} = -(a + b\, r)$$

$$s_{23} = A - B(r\, v + \sqrt{1 - r^2}\, \sqrt{1 - v^2}\, \cos\gamma)$$

$$a = \frac{(s_{12} + m_a^2 - t_{23})(s_{12} + m_1^2 - m_2^2)}{2s_{12}} - m_a^2 - m_1^2$$

$$b = \frac{\sqrt{\lambda(s_{12}, m_a^2, t_{12})}\, \lambda(s_{12}, m_1^2, m_2^2)}{2\, s_{12}}$$

$$v \equiv \hat{q}_a \cdot \hat{q}_3 = \frac{(s_{12}+m_a^2-t_{12})(s-s_{12}-m_3^2)-2s_{12}(s+t_{23}-m_b^2-s_{12})}{\sqrt{\lambda(s, s_{12}, m_3^2)}\, \lambda(s_{12}, m_a^2, t_{23})} \qquad \text{(III. 23)}$$

where A, B are defined by Eq. (III. 16). The cross section comes from Eq. (III. 9) with the above ρ_3. If $\alpha_2(t_{23})$ is an integer, as would be the case for a trajectory corresponding to a Kronecker delta in the angular momentum plane, then the integration over r can be done analytically. Otherwise, all three integrations must be done by machine to obtain the $d\sigma_3/d\gamma$ distribution. Cuts in s_{23}, t_{12} will

affect the r integration limits as seen in Eq. (III.23). The limits of the s_{12}, t_{23} integrations are controlled by the Chew-Low plot boundaries and cuts in these variables.

5. Middle Mass Distribution

In a given reaction at fixed beam energy, different particles can be produced at the middle vertex. Multi-Regge dynamics depend on the particle produced through the allowed exchanges and the coupling at the middle vertex. Therefore, a distribution of the cross section as a function of the middle particle's mass can provide information about the middle vertex. This distribution is easily obtained from the previously discussed $d\sigma_3/ds_{ij}$ distribution by integrating over s_{ij}. The resulting cross section can be plotted versus m_2 (the middle particle mass) to give the desired distribution.

D. Fitting Procedure

The most striking features seen in experimental momentum transfer and subenergy distributions are the fall-off rates of the cross section with increasing t and s respectively. We know from the theoretical distributions just discussed that trajectory slopes, exponential factors, and Regge intercepts most strongly affect these rates. The problem, then, is to determine these parameters and check their consistency with two body values. For a more detailed theory and with increased statistics, a least squares fit should give a meaningful quantitative (in the χ^2 sense) parameter determination, but the present state of the multi-Regge theory and our low statistics limit us to a good qualitative fit to the data.

The fitting procedure we employ is outlined in Chapter IV for the particular reaction analyzed there. We should point out that the trajectory slopes need not be assumed as is done in that analysis, but could be determined by a quantitative fit. The difficulty occurs because the slopes α_i' always enter the amplitude in the form $c_i + \alpha_i' \ln s_{i,i+1}$, so, consequently, a change in α_i' cannot be separated from one in the exponential factor c_i except through the slow logarithmic variation in $s_{i,i+1}$. Our qualitative fit is insufficiently sensitive to determine values of α_i', so we fixed them at their two body values.

CHAPTER IV

Multi-Regge Analysis of a Particular Reaction

We now apply the analysis described in Chapter III to the particular reactions

$$\pi^- + p \rightarrow \pi^- + X + p \qquad \text{(IV. 1)}$$

$$X \rightarrow \pi^- \pi^+ \qquad \text{(IV. 2)}$$

at an incident π^- energy of 25 BeV[18]. The events were selected from an 80 - in. bubble-chamber exposure at the Brookhaven National Laboratory by the Walker-Erwin group at the University of Wisconsin. In analyzing the reaction, we always work in a kinematic region where the theoretical assumptions leading to the multi-Regge form for the amplitude are kept to a minimum. Simultaneous with the requirement that the p and π^- momentum transfers be small, we demand that all invariant masses (except that of the X) be large. This is the first time this particular kinematic region has been investigated experimentally. The consistency of the multi-Regge hypothesis has been previously investigated by several groups[15, 19], but always in kinematic regions where the validity of application is uncertain and additional assumptions are involved[20].

We now change the notation of Chapter III slightly to facilitate discussion of reactions (IV. 1) and (IV. 2) . We treat X as a stable particle of definite mass. The two momentum transfers t_{12} and t_{23} become $t_\pi = (\pi_f - \pi_i)^2$ and $t_p = (p_f - p_i)^2$ respectively, while the final state invariant masses s_{12} and s_{23} become $s_{\pi X} = (\pi_f + X)^2$

and $s_{Xp} = (X + p_f)^2$ respectively. Here the particle symbol stands for the four vector of that particle, while the subscripts "i" and "f" denote "initial" and "final" (figure 7(a)). Equation (III.4) gives for the multi-Regge amplitude

$$A \sim \beta_{\pi\alpha_1\pi}(t_\pi)\zeta_1(t_\pi)s_{\pi X}^{\alpha_1(t_\pi)}\gamma_{\alpha_1 X\alpha_2}(t_\pi, \omega, t_p)s_{Xp}^{\alpha_2(t_p)}\zeta_2(t_p)\beta_{p\alpha_2 p}(t_p) \qquad \text{(IV. 3)}$$

where the notation for the residues defined there has been altered for convenience.

The primary object of the chapter is to demonstrate that the data are consistent with multi-Regge exchange if $\alpha_1(0) \approx \frac{1}{2}$, $\alpha_2(0) \approx 1$. This indicates that if the isospin I of the X is 1, ρ and Pomeranchon (P) exchange are most important; while if the X has I = 0, the P' and P may be dominant contributors. The data clearly exclude double-Pomeranchon exchange as the dominant production mechanism for reaction (IV. 1). If the (I = 0)/(I = 1) X production ratio is small, then the I = 0 X may still be produced primarily via double-P exchange.

We now turn to the problem of cuts in the data. The five types of restrictions listed in Chapter III, Part B are imposed on reaction (IV. 1). We treat these restrictions in the same order here.

There is, in general, an ambiguity as to whether a particular π^- should be grouped with the π^+ to form an X, or whether it should be called π_f^-. We take π_f^- to be, by definition, that π^- which makes the smallest momentum transfer with the incident π^-, i.e.,

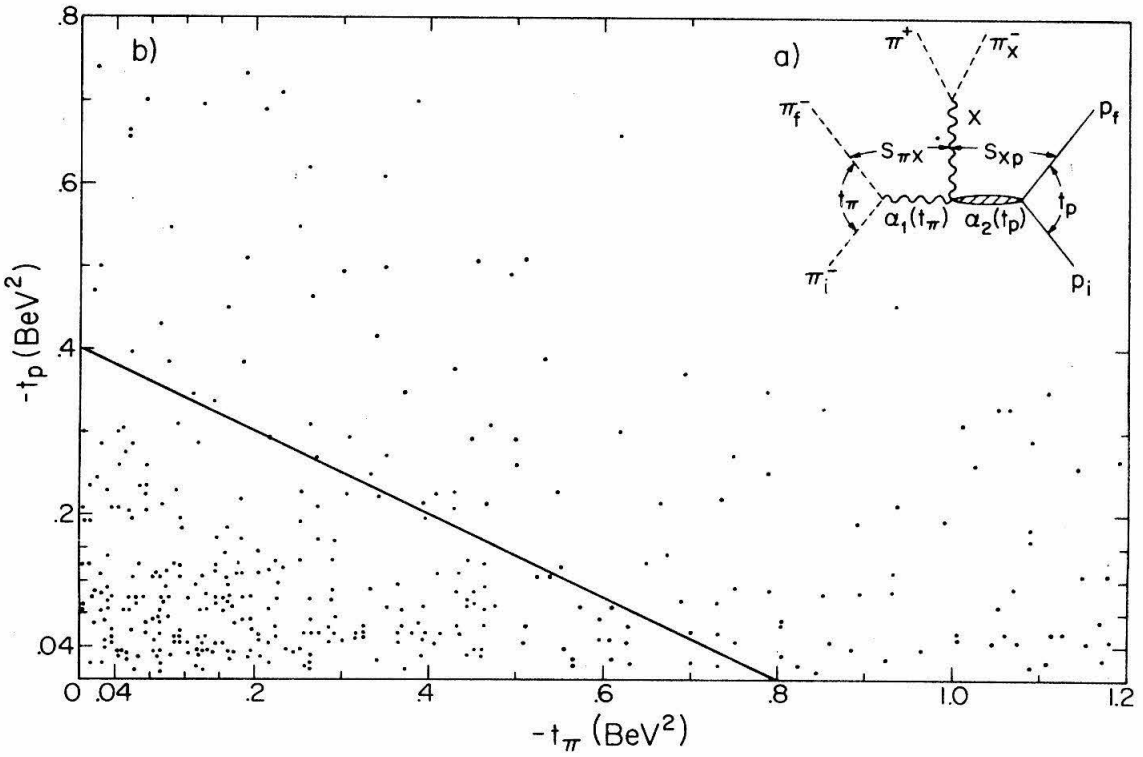

Figure 7. (a) Particles, trajectories, and variables for the reactions studied.

(b) t_π-t_p scatter plot. The line $|t_\pi+2t_p| = 0.8$ is used in making a momentum-transfer cut of the data. To the scale shown, the kinematic boundaries are given by the lines $t_p = 0$ and $t_\pi = 0$. Contrast this experimental distribution with phase space predictions of figure (4).

$$|(\pi_f^- - \pi_i^-)^2| = |t_\pi| < |(\pi_X^- - \pi_i^-)^2| \ ,$$

where π_X^- designates the π^- that is included in X.

We have indicated that Eq. (IV. 3) is expected to hold when both final-state invariant masses are large, while both momentum transfers are small. More precisely, we shall restrict ourselves to events where $s_{\pi X}$ and s_{Xp} lie outside the final-state two-body resonance region, i. e.,

$$s_{\pi X} \geq 2 \text{ BeV}^2 \ (40\%), \quad s_{Xp} \geq 4 \text{ BeV}^2 \ (25\%) \ ,$$

$$s_{\pi p} = (\pi_f + p_f)^2 \geq 4 \text{ BeV}^2 \ (2\%) \ . \qquad \text{(a)}$$

The percentage indicates the fraction of events that are removed, at each stage, as a result of the cut employed; we begin with ~2000 four-prong, four-constraint events with identifiable proton. Our results are insensitive to the exact location of these, and subsequent, cuts. The momentum-transfer constraints will be described shortly. Other investigators[15] have not required that both final-state invariant masses be large. Justification for this must rest on some, as yet ill-defined, generalization of Dolen-Horn-Schmid "duality" to multiparticle amplitudes.[20] Since this "duality" principle frequently does not work in two-body reactions when we include only one or two trajectories,[21] we feel that if we want to demonstrate the validity of Eq. (IV. 3), we had best work in kinematic regions which are free of "duality" uncertainties.

When the X mass is large (above the $\pi^+\pi_X^-$ resonance region), the dynamics presumably are described by triple-Regge exchange. Since the number of events here is small, we ignore these for sim-

plicity and confine ourselves to the double-Regge-exchange region by requiring

$$m_X^2 = (\pi^+ + \pi_X^-)^2 \leq 2 \text{ BeV}^2 \ (8\%) , \qquad \text{(b)}$$

except for X = g(1.650 BeV).

We have, in addition, removed those events where one of the π's from the X resonates with either the final proton or π^-, i.e.[22],

$$(\pi^+ + p_f)^2 \neq m_\Delta^2 \ (18\%) ,$$

$$(\pi^+ + \pi_f^-)^2 \neq m_\rho^2, \ m_f^2 \ (31\%) . \qquad \text{(c)}$$

In order to see if our data are consistent with MRE, we first look for an accumulation of events [satisfying (a) - (c)] when the momentum transfers t_π and t_p are both simultaneously small. This is one of the most striking features contained in Eq. (IV.3) (exponentials in momentum transfer arise both from the β's and the s^α factors), and will determine if a multiperipheral signal is present in the data when the final-state invariant masses $s_{\pi X}$ and s_{Xp} are both large. The result is shown on a t_π - t_p plot in figure 7(b). Note that there is a large excess of events when both t's are small even though phase space vanishes at the boundaries of this plot. We now isolate this multiperipheral signal by restricting ourselves to the small momentum-transfer events contained within the region

$$|t_\pi + 2t_p| \leq 0.8 \text{ BeV}^2 \ (40\%) , \qquad \text{(d)}$$

and examine them to see if they are consistent with the expected detailed MRE structure. We have not treated t_p and t_π symmetrically in (d) because the peaking in t_p is sharper than the peaking in t_π. This asymmetry is our first indication that double-P exchange is not dominant. Double-P exchange would require all distributions for Reaction (IV. 1) to be approximately symmetric under the interchange $t_\pi \leftrightarrow t_p$ [recall that πp and pp elastic scattering have similar diffraction peak slopes implying, via factorization, that $\beta_{\pi\alpha_p\pi}(t) \approx \beta_{p\alpha_p p}(t)$]. Note that earlier analysis[15,19] did not incorporate this type of momentum-transfer cut (d). We have found it useful in sharpening the MRE signal.

The cross section for the 250 events which remain after the application of conditions (a) - (d) is 95 ± 10 μb.

We now make the assumptions (a) - (e) of Chapter III, Part C to obtain the explicit multi-Regge amplitude of equation (III. 8).

To obtain some feeling for the relative size of $\alpha_1(t)$ and $\alpha_2(t)$, we examine the $s_{\pi X}$ and s_{Xp} distributions [figures 8(c) and 8(d)]. The differences in scale are striking. Approximately half the events have $s_{Xp} > 15$ BeV^2; there are no events with $s_{\pi X} > 15$ BeV^2. This asymmetry automatically excludes dominant double-P exchange and implies $\alpha_1(t) < \alpha_2(t)$ in the small-t region under investigation.

We now come to the fitting procedure mentioned in Chapter III, Part D. For the reasons listed there we carry out a qualitative fitting scheme instead of an unfeasible least squares routine.

In this analysis we will not attempt a determination of $\alpha_1'(0)$ and $\alpha_2'(0)$; anticipating the fits we will obtain (i.e., 1 = ρ or P', 2 = P) we shall take these as inputs to be 1/BeV^2 and 0, respectively.

We first guess that $\alpha_1(0) \approx 1/2$, $\alpha_2(0) \approx 1$, and $c_2 \approx 5$, being guided by our knowledge of two-body reactions and our expectation that 1 = ρ or P', 2 = P (we know $b_2 \approx 2.5$ and we might expect a comparable value for g_2). The results of performing the integrations to obtain the t_π distribution are shown in figure 8(a), and favor $c_1 \approx 1$. The next step is to take $\alpha_1(0) \approx 1/2$, $\alpha_2(0) \approx 1$, and $c_1 \approx 1$, and to fit c_2 with a t_p plot as shown in figure 8(b). Note that $c_2 \approx 5$ works quite well although the first t_p bin appears somewhat underpopulated. Fixing $c_1 \approx 1$, $c_2 \approx 5$, we now fit $\alpha_1(0)$ and $\alpha_2(0)$ from the $s_{\pi X}$ and s_{Xp} distributions [figures 8(c) and 8(d)]. As stated previously, the s-distributions depend rather critically on both $\alpha_1(0)$ and $\alpha_2(0)$. For example, in the s_{Xp} distribution, high values of s_{Xp} depend most sensitively on $\alpha_2(0)$, as expected, but low values depend both on $\alpha_1(0)$ and $\alpha_2(0)$. A consistent fit to the qualitative features of both s distributions is found with $\alpha_1(0) \approx 1/2$, $\alpha_2(0) \approx 1$, in agreement with the predictions of MRE if 1 = ρ or P', 2 = P (recall that the ρ and P' trajectories have comparable intercepts at t = 0).

Although our s_{Xp} fit [curve A, figure 8(c)] works quite well for large values of s_{Xp}, there are definite discrepancies at low s_{Xp}. These can be corrected, without altering the goodness of fit to the other three distributions, by adding in a small contribution with $\alpha_1(0) \approx 1$, $\alpha_2(0) \approx 1/2$ and allowing it to interfere with the main term in the amplitude.[23]

Identifying 2 = P, taking $c_P \approx 5$ from our analysis, and using $b_P \approx 2.5$ from two-body reactions, we have $g_P \approx 2.5$. Since b_1 is essentially unknown, we are unable to estimate g_1.

We now check our assumption of the independence of γ on ω by computing the expected ω distribution and comparing it with

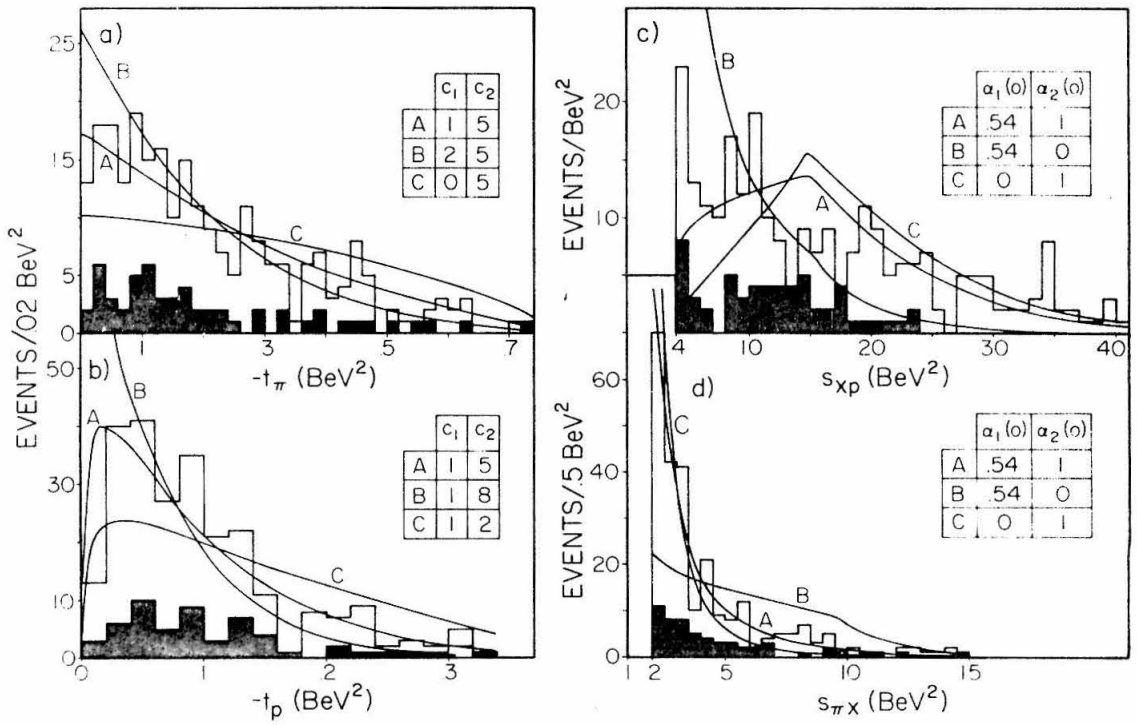

Figure 8. (a)-(d) t_π, t_p, s_{Xp}, and $s_{\pi X}$ distributions, respectively. Note scale changes. The shaded events in this and succeeding graphs correspond to 0.7 BeV < M_X < 0.83 BeV, where M_X is the mass of the X. Only about 1/3 of these events are actual ρ's. To simplify the calculations, the theoretical curves were computed assuming an average X mass equal to 0.765 BeV.

experiment [figure 9(b)]. Note the fit is satisfactory; no variation of γ with ω is needed.

To understand what comprises X, we have plotted the invariant X mass for events which satisfy all constraints except (b). Note that while some ρ is present ($\sim$20 events), no strong f (< 15 events) or g (< 3 events) signal is observed.[24] Since the g lies on the same trajectory as the ρ, the difference between g and ρ production may be attributed solely to differences in γ and phase space factors. Phase space favors g over ρ by a factor of 4 [solid line, figure 9(a)]. Consequently, the middle residue γ must fall dramatically as we move along the X trajectory from ρ to g. We have estimated theoretically the f/ρ production cross-section ratio to be 25 assuming $\alpha_1 = \alpha_P$, $\alpha_2 = \alpha_P$ for f, $\alpha_1 = \alpha_\rho$, $\alpha_2 = \alpha_P$ for ρ, and $\gamma_{\alpha_P f \alpha_P} = \gamma_{\alpha_\rho \rho \alpha_P}$. Since the experimental f/ρ production ratio is ≤ 1, we have additional evidence that double-Pomeranchon exchange is either severely suppressed or absent.

In summary, we have found that (1) multiperipheral events exist even when final-state invariant masses are large. (2) The multiperipheral events are consistent with a MRE structure. We find $\alpha_P(0) \approx 1$, $\alpha_\rho(0) \approx 1/2$, and/or $\alpha_{P'}(0) \approx 1/2$, in good agreement with determinations of these parameters from two-body reactions. Double-Pomeranchon exchange is not dominant. (3) The internal vertex γ is independent of the angle ω. (4) Multiperipheral f production is suppressed by a factor of at least 25 over what one might expect from double-Pomeranchon exchange. (5) Multiperipheral g production is small indicating that residues considered as functions of external mass are strongly damped with increasing mass. (6) The cross section for the MRE events is 95 $\pm$ 10 μb. We have used the

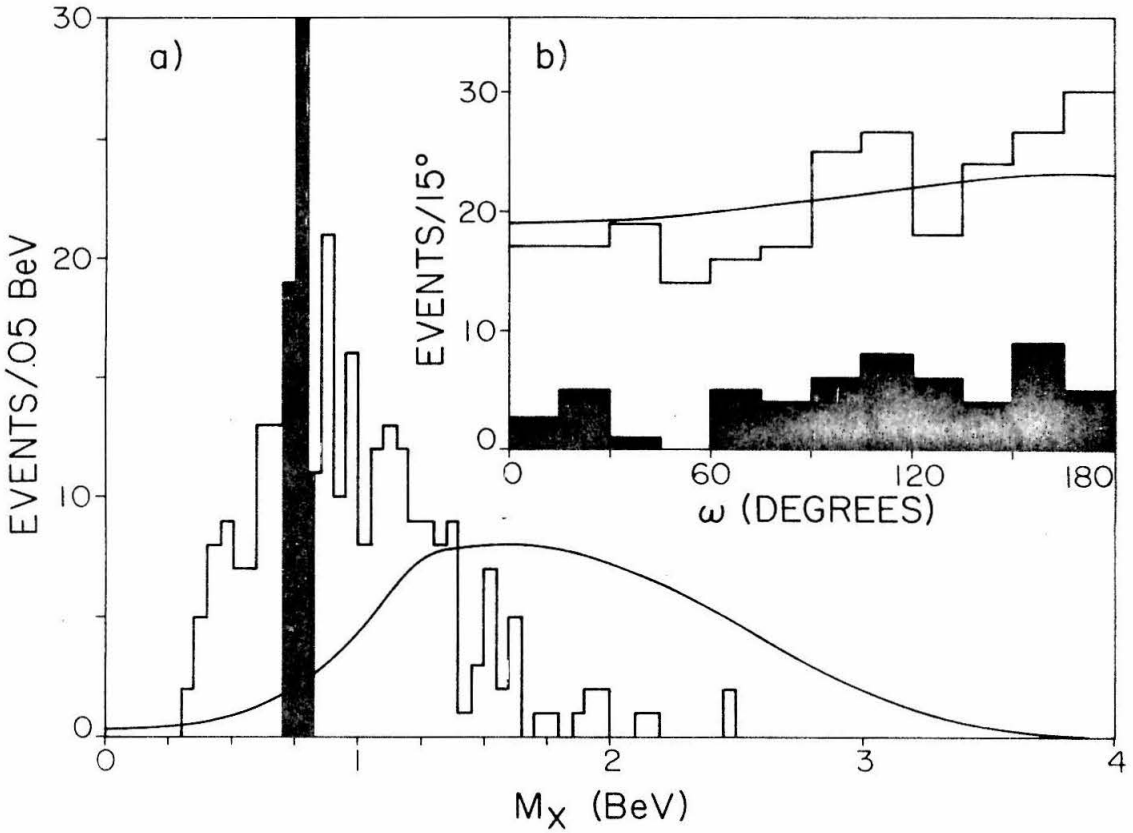

Figure 9. (a) X invariant-mass plot. The solid line is obtained from Eq. (IV.3) assuming $\gamma_{\alpha_1 X \alpha_2}$ is independent of X.

(b) ω angular distribution. The solid curve follows from Eq. (IV. 3) assuming $\gamma_{\alpha_1 X \alpha_2}$ is independent of ω .

MRE model, normalized to this cross section, to predict cross sections for this same reaction at other energies. We find that the cross section peaks at around 10 BeV with a maximum value of ~165 μb. However, at this low energy, ambiguities in grouping the final-state particles may become serious.

CHAPTER V

Cross Section Estimates in the Multi-Regge Model

We can use the multi-Regge model to predict the cross section of various production processes. The assumptions necessary to obtain an explicit form for the amplitude, along with our ignorance of some Regge coupling strengths limit the accuracy of these predictions, but should not affect their qualitative features. The resulting cross sections can give us a rough idea of the accessibility of these reactions to experimental investigation, and, hence, may prove useful in preliminary planning stages of experiments to test the multi-Regge hypothesis.

We consider only three body final states, although one of the final particles may be a resonance. We integrate the explicit form of the amplitude, given by Eq. (III. 8), over all variables except overall s. For the external Regge residues, we assume

$$\beta_{a\alpha_1 1}(t_{12}) = \Gamma_{a\alpha_1 1} e^{-b_1 t_{12}} \qquad \text{(V. 1)}$$

$$\beta_{b\alpha_2 3}(t_{23}) = \Gamma_{b\alpha_2 3} e^{-b_2 t_{23}} \qquad \text{(V. 2)}$$

where we obtain the b's from differential cross sections and the Γ's from total cross sections in two body reactions. For the middle vertex we assume

$$\gamma_2(t_{12}, \omega, t_{23}) = \Gamma_2 e^{g_1 t_{12} + g_2 t_{23}} . \qquad \text{(V. 3)}$$

The g_i are completely unknown, but we might expect that they do not differ too greatly from the b_i, so we try $g_i = b_i = c_i/2$, $i = 1, 2$. We take Γ_2 the same for all reactions, fixing its value by the reactions (IV. 1 , IV. 2) for which the cross section is 95 ± 10 μb at a laboratory momentum of 25 BeV/c.

We present the results in tabular form. Tables I and II list the values of the Regge parameters used in the calculations[25,26,27,28]. Table III lists the resulting cross sections normalized as mentioned above. No interference effects between amplitudes with different Regge exchanges have been included.

We conclude with the following comments:

(a) As in two body interactions, the relative importance of contributing trajectories is determined by their intercepts.

(b) For fixed laboratory momentum, the cross section increases with the middle particle mass until the allowable phase space is exhausted.

(c) The reaction $\pi N \rightarrow \pi X N$ where the X has isospin zero theoretically has the largest cross section since double-Pomeranchon exchange is allowed. The results of Chapter IV demonstrate, however, that double-P exchange is not present to any appreciable extent. Thus, the $\pi N \rightarrow \pi X N$ cross section where X has isospin one, even though theoretically 22 times smaller than isospin zero cross section, is expected to be largest experimentally. This means reactions (IV. 1, IV. 2) probably represent an upper limit of the multi-Regge signal at this energy.

TABLE I

Regge Trajectory Parameters

Trajectory $\alpha(t)$	Intercept $\alpha(0)$	Slope $\alpha'(0)$ (BeV^{-1})	Exponential Factor $c(BeV^{-1})$
Pomeranchon P	1	0	5
Rho ρ	.54	1	2
Nucleon N	-.39	.74	3
Delta (1236) Δ	.24	.56	0

TABLE II

Regge Residue Moduli

Trajectory	External Particles	Γ
Pomeranchon P	π, π	1.39
	N, N	1.56
Rho ρ	π, π	1.16
	N, N	0.95*
Nucleon N	π, N	1.39
Delta (1236) Δ	π, N	0.45

*Reference (25)states that this residue is consistent with zero, but 0.95 represents its upper limit.

TABLE III

Calculated Cross Sections

Reaction	Trajectory 1	Trajectory 2	Cross Section (μb)
1. $\pi N \to \pi X N$	ρ	P	95
where X has I=1	P	ρ	37
	ρ	ρ	7
2. $\pi N \to \pi X N$	P	P	208
where X has I=0			
3. $NN \to N \pi N$	ρ	ρ	0.6
4. $NN \to N X N$	ρ	P	41
where X has I=1	ρ	ρ	32
5. $NN \to \pi NN$	N	P	56
6. $\pi N \to \pi N \pi$	P	N	40
7. $\pi N \to \pi \Delta \pi$	P	Δ	67

APPENDIX A

Toller Variables

I. Introduction

In attempting to generalize the partial wave analysis of the scattering amplitude Setorio and Toller[29,30] have introduced a set of variables that appears useful for describing high energy processes, particularly those in which multi-Regge behavior may be present. The usual partial wave analysis decomposes the scattering amplitude into irreducible representations of a subgroup of the Lorentz group, namely the group of spatial rotations. The rotation group can be characterized as the subgroup of the Lorentz group that leaves a pure timelike vector invariant. Toller concerns himself with the subgroup of the Lorentz group that leaves a pure spacelike vector invariant. This subgroup operates on vectors with one timelike and two spacelike dimensions; its properties have been thoroughly investigated by Bargmann[31]. The 2×2 matrix representations of this subgroup are of the form

$$M(g) = \begin{pmatrix} a & b \\ b^* & a^* \end{pmatrix} \text{ with } aa^* - bb^* = 1 \qquad \text{(A. 1)}$$

where g is an element of the subgroup. They can be parameterized with the variables μ, ξ, ν through

$$M(g) = \begin{pmatrix} e^{+i\mu/2} & 0 \\ 0 & e^{-i\mu/2} \end{pmatrix} \begin{pmatrix} \text{COSH } \xi/2 & \text{SINH } \xi/2 \\ \text{SINH } \xi/2 & \text{COSH } \xi/2 \end{pmatrix} \begin{pmatrix} e^{+i\nu/2} & 0 \\ 0 & e^{-i\nu/2} \end{pmatrix} \qquad \text{(A. 2)}$$

where $0 \leq \mu \leq 2\pi$, $0 \leq \xi < \infty$, $0 \leq \nu \leq 2\pi$. As usual a four vector $V = (t, x, y, z)$ transforms according to $V \to V' = MVM^{\dagger}$, or

$$\begin{pmatrix} t' + z' & x' - iy' \\ x' + iy' & t' - z' \end{pmatrix} = \begin{pmatrix} a & b \\ b^* & a^* \end{pmatrix} \begin{pmatrix} t + z & x - iy \\ x + iy & t - z \end{pmatrix} \begin{pmatrix} a^* & b \\ b^* & a \end{pmatrix} . \qquad (A.3)$$

Thus, in a 4×4 representation $L(g)$, for which $V' = L(g)V$ is

$$L(g) = \begin{pmatrix} 1 & 0 & 0 & 0 \\ 0 & \text{COS}\,\mu & +\text{SIN}\,\mu & 0 \\ 0 & -\text{SIN}\,\mu & \text{COS}\,\mu & 0 \\ 0 & 0 & 0 & 1 \end{pmatrix} \begin{pmatrix} \text{COSH}\,\xi & \text{SINH}\,\xi & 0 & 0 \\ \text{SINH}\,\xi & \text{COSH}\,\xi & 0 & 0 \\ 0 & 0 & 1 & 0 \\ 0 & 0 & 0 & 1 \end{pmatrix}$$

$$\times \begin{pmatrix} 1 & 0 & 0 & 0 \\ 0 & \text{COS}\,\nu & +\text{SIN}\,\nu & 0 \\ 0 & -\text{SIN}\,\nu & \text{COS}\,\nu & 0 \\ 0 & 0 & 0 & 1 \end{pmatrix} . \qquad (A.4)$$

As required, the z component of V is left invariant.

II. Toller Variables

To illustrate the use of these variables in a scattering process we will assume we have two particles scattering into N particles. Following Bali, Chew, Pignotti[32], we divide the N particles into two clusters of N_1 and N_2 particles ($N_1 + N_2 = N$), and label the particles' four momenta as shown in figure 10. We assume energy-momentum conservation at all vertices, and that q_a, $q_{N_1+1}, \ldots, q_N$

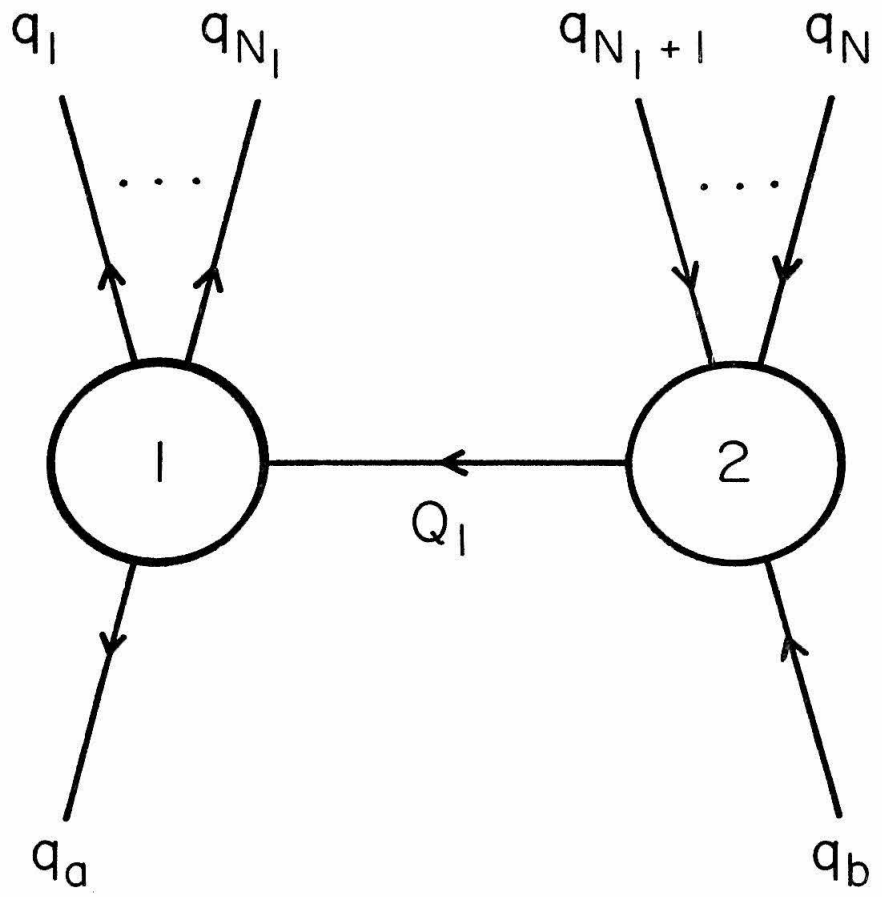

Figure 10. Particle four momenta for two cluster break-up.

all have negative energies. As shown at the beginning of Chapter II, the process can be described by $3(N + 2) - 10$ parameters. Comprising these parameters are:

(1) one invariant momentum transfer $Q_1^2 \equiv t_{12}$.

(2) $3(N_1 + 2) - 10$ internal variables associated with cluster 1

(3) $3(N_2 + 2) - 10$ internal variables associated with cluster 2

(4) 3 variables characterizing Lorentz transformations of cluster 1 relative to cluster 2 that leave four vector Q_{12} invariant.

We restrict ourselves to physical scattering situations in which Q_1 will be spacelike. Then, the three variables mentioned in (4) become the μ, ξ, ν of Eq. (A. 2), (A. 4). As a matter of convention, we associate two standard frames with Q_1. The frame (1, ℓ) has Q_1 pure spacelike, $\vec{q}_a$ directed along the z-direction, and $\vec{q}_1$ contained in the x-z plane with a positive x component. The frame (1, r) has Q_1 pure spacelike, $\vec{q}_b$ directed along the z axis, and $\vec{q}_{N_1+1}$ contained in the x-z plane with a positive x component. The "ℓ" or "r" in the designation means that the momentum with only a spatial z component is to the left or the right of Q_1 as seen in figure 10. In frame (1, ℓ), the four vectors have the form

$$q_a = [-(m_a^2 + q_{az}^2)^{1/2},\ 0,\ 0,\ q_{az}]$$

$$q_1 = [-(m_1^2 + q_{1x}^2 + q_{1z}^2)^{1/2},\ q_{1x} \geq 0,\ 0,\ q_{1z}]$$

$$Q_1 = [0,\ 0,\ 0,\ \sqrt{-t_{12}}\ ] \ . \qquad \text{(A. 5)}$$

In frame (1, r), q_b and q_{N_1+1} have analogous forms. We can reach frame (1, r) from frame (1, ℓ) by a suitable Lorentz transformation

that leaves Q_1 invariant. The transformation consists in rotating about the z-axis until the x-axis lies in the plane of $\vec{Q}_1$ and $\vec{q}_b$, then boosting in this direction until $\vec{q}_b$ has only a z component, and finally rotating about the z-axis until the x-axis lies in the plane of $\vec{Q}_1$ and $\vec{q}_{N_1+1}$. If the rotation angles are μ_{12} and ν_{12} respectively, and the boost is of magnitude ξ_{12}, any four vector V in (1, r) becomes in (1, ℓ) :

$$V(1, \ell) = L(\mu_{12}, \xi_{12}, \nu_{12})\, V(1, r) \equiv L(g_{12})\, V(1, r) \qquad (A.6)$$

where $L(g_{12})$ is represented by the matrix of Eq. (A.4). For illustration we can compute the overall center of mass energy

$$S_{ab} = (q_a - q_b)^2 = m_a^2 + m_b^2 - 2q_a \cdot q_b$$

$$q_b(1, \ell) = L(g_{12})\, q_b(1, r) = \begin{pmatrix} 1 & 0 & 0 & 0 \\ 0 & \text{COS}\mu_{12} & +\text{SIN}\mu_{12} & 0 \\ 0 & -\text{SIN}\mu_{12} & \text{COS}\mu_{12} & 0 \\ 0 & 0 & 0 & 1 \end{pmatrix} \begin{pmatrix} \text{COSH}\,\xi_{12}\ E_b \\ \text{SINH}\,\xi_{12}\ E_b \\ 0 \\ q_b \end{pmatrix}$$

$$= \begin{pmatrix} \text{COSH}\,\xi_{12} & E_b \\ \text{SINH}\,\xi_{12} & \text{COS}\mu_{12}\ E_b \\ -\text{SINH}\,\xi_{12} & \text{SIN}\,\mu_{12}\ E_b \\ & q_b \end{pmatrix} . \qquad (A.7)$$

Thus, $S_{ab} = m_a^2 + m_b^2 + 2E_aE_b\ \text{COSH}\,\xi_{12} + 2q_aq_b$, so the center of mass energy squared is linearly related to $\text{COSH}\,\xi_{12}$. To understand this relationship better, we express the energies and moments in

terms of invariants. Let $V_1 = \sum_{i=1}^{N_1} q_i$ and $V_2 = \sum_{i=N_1+1}^{N} q_i$, so $|\vec{V}_1| + q_a = |\vec{V}_2| + q_b = \sqrt{-t_{12}}$ and $V_{10} + E_1 = V_{20} + E_2 = 0$. Therefore

$$q_a = -\frac{t_{12} + m_a^2 - V_1^2}{2\sqrt{-t_{12}}}, \quad E_a = \frac{\sqrt{\lambda}(t_{12}, m_a^2, V_1^2)}{2\sqrt{-t_{12}}}$$

$$q_b = -\frac{t_{12} + m_b^2 - V_2^2}{2\sqrt{-t_{12}}}, \quad E_b = \frac{\sqrt{\lambda}(t_{12}, m_b^2, V_2^2)}{2\sqrt{-t_{12}}} \cdot \qquad \text{(A.8)}$$

Notice, though, that if we had computed $(q_a - q_b)^2$ in the t-channel center of mass frame (Q_{12} timelike), we would have obtained

$$S_{ab} = m_a^2 + m_b^2 - \frac{(t_{12} + m_a^2 - V_1^2)(t_{12} + m_b^2 - V_2^2)}{2t_{12}} + \frac{\sqrt{\lambda}(t_{12}, m_a^2, V_1^2)\,\lambda(t_{12}, m_b^2, V_2^2)}{2t_{12}} \text{COS}\,\theta_t \qquad \text{(A.9)}$$

where θ_t is the angle between $\vec{q}_a$ and $\vec{q}_b$. Comparing Eq. (A.9) with the equation for S_{ab} expressed in Toller variables, we see that COSH ξ_{12} is the analytic continuation of the cross channel cosine, i.e., $\theta_t \to i\,\xi_{12}$ as one goes from the t to the s channels.

III. Cases with Multiple Clusters

Consider the general case of M clusters with N final particles shown in figure 11. The q_i represent the sum of all final momenta in cluster i. We assume each Q_i, the momentum transfer to the right of cluster i, is spacelike. We generalize the convention of the two cluster case to define frames (i, ℓ) and (i, r). In frame (i, ℓ) Q_i is pure spacelike, $\vec{Q}_{i-1}$ is directed along the z-direction, and $\vec{q}_i^{(1)}$, the spatial momentum of an arbitrarily designated final particle of cluster i, is contained in the x-z plane with positive x component. An analogous definition of frame (i, r) is made. The fact that Q_{i-1} and Q_{i+1} are spacelike, whereas, the corresponding q_a and q_b in the two cluster case were timelike causes no problem. The Lorentz transformation from frame (i, ℓ) to frame (i, r) which leaves Q_i invariant and involves Toller variables $\mu_{i, i+1}$, $\xi_{i, i+1}$, $\nu_{i, i+1}$, we denote by $L(\mu_{i, i+1}, \xi_{i, i+1}, \nu_{i, i+1}) \equiv L(g_{i, i+1})$. The Lorentz transformation from frame $(i-1, r)$ to frame (i, ℓ) involves a boost in the z-direction. Before the transformation $Q_i = (\sqrt{t_{i, i+1} + z_{i, i+1}^2}, 0, 0, z_{i, i+1} > 0)$, while after the boost $Q_i = (0, 0, 0, \sqrt{-t_{i, i+1}})$. Parameterizing the boost by γ_i, we have

$$\text{COSH } \gamma_i = \frac{z_{i, i+1}}{\sqrt{-t_{i, i+1}}} = \frac{q_i^2 - t_{i-1, i} - t_{i, i+1}}{2\sqrt{-t_{i-1, i}}\sqrt{-t_{i, i+1}}} \qquad \text{(A. 10)}$$

where q_i^2 is the invariant mass squared of cluster i. This Lorentz boost, denoted by $L(\gamma_i)$, leaves all momenta of cluster i in standard form.

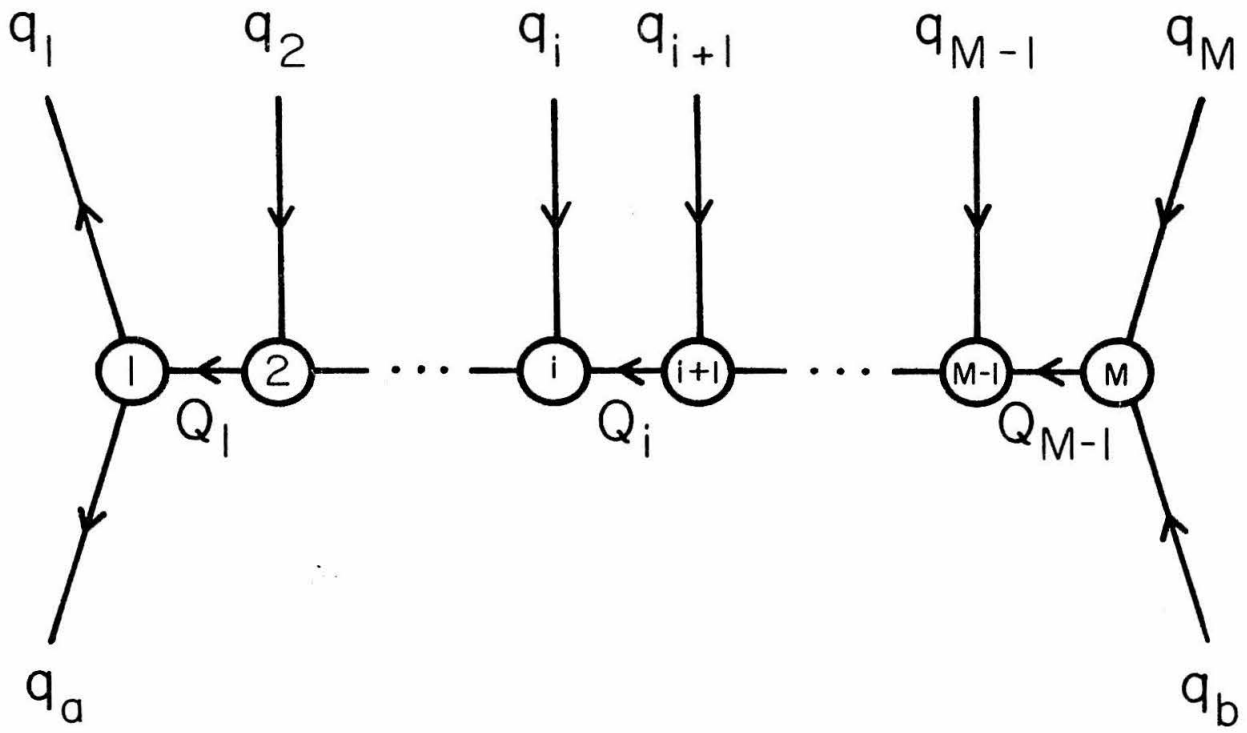

Figure 11. Particle four momenta for multi-cluster break-up.

For multiple clusters, the 3N-4 parameters of the process are M-1 momentum transfers, 3(M-1) Toller variables, and $\sum_{i=1}^{M} (3N_i - 4) = 3N - 4M$ internal variables from the M clusters. Although, the Toller variables are defined in different Lorentz frames, successive applications of the operation $L(\gamma_i)$ and $L(g_{i,i+1})$ allow us to express all four momenta in a common frame, and, thus, to relate these variables to invariants. For example, a particle from cluster i has the standard form in frame (i,ℓ). In frame $(1,\ell)$, its four vector K becomes

$$K(1,\ell) = L(g_{12})L(\gamma_2)L(g_{23}) \ldots L(\gamma_{i-1})L(g_{i-1,i})L(\gamma_i)\, K(i,\ell) . \tag{A. 11}$$

The above analysis applies when each cluster has more than one particle. In frame (i-1, r), the angle $\nu_{i-1,i}$ is defined by

$$\cos \nu_{i,i+1} = \frac{(\vec{Q}_{i-1} \times \vec{q}_i^{(1)})}{|\vec{Q}_{i-1} \times \vec{q}_i^{(1)}|} \cdot \frac{(\vec{Q}_{i-2} \times \vec{Q}_{i-1})}{|\vec{Q}_{i-2} \times \vec{Q}_{i-1}|} . \tag{A. 12}$$

In the frame (i,ℓ), the angle $\mu_{i,i+1}$ is defined by

$$\cos \mu_{i,i+1} = \frac{(\vec{Q}_i \times \vec{Q}_{i+1})}{|\vec{Q}_i \times \vec{Q}_{i+1}|} \cdot \frac{(\vec{Q}_i \times \vec{q}_i^{(1)})}{|\vec{Q}_i \times \vec{q}_i^{(1)}|} \tag{A. 13}$$

where $q_i^{(1)}$ is the four momentum of the final particle of cluster i designated to have no x component in standard form. Both $\nu_{i-1,i}$ and $\mu_{i,i+1}$ are well defined when cluster i has two or more particles.

But, when cluster i has one final particle, $q_i^{(1)} = Q_{i-1} - Q_i$. In frames (i-1, r) and (i, ℓ), Q_{i-1} and Q_i both have only a z component of spatial momentum, hence, $\vec{q}_i^{(1)} \times \vec{Q}_{i-1} = \vec{q}_i^{(1)} \times \vec{Q}_i = 0$ in both frames, so $\nu_{i-1,\,i}$ and $\mu_{i,\,i+1}$ are not defined. The amplitude cannot depend on both $\nu_{i-1,\,i}$ and $\mu_{i,\,i+1}$, but only on their sum $\omega_i \equiv (\nu_{i-1,\,i} + \mu_{i,\,i+1})$. In frames (i-1, r), (i, ℓ), or any frames reached from these by a z-direction boost

$$\text{COS}\ \omega_i = \frac{(\vec{Q}_i \times \vec{Q}_{i-2})}{|\vec{Q}_i \times \vec{Q}_{i-2}|} \cdot \frac{(\vec{Q}_{i+1} \times \vec{Q}_i)}{|\vec{Q}_{i+1} \times \vec{Q}_i|} \cdot \qquad \text{(A. 14)}$$

If a cluster has only particle, formally it has 3(1) - 4 = -1 internal variables, which can be interpreted to mean the removal of one of the Toller variables, i. e., $\nu_{i-1,\,i}$, $\mu_{i,\,i+1} \rightarrow \omega_i = \nu_{i-1,\,i} + \mu_{i,\,i+1}$. With this interpretation all the formulae concerning the distribution of independent parameters remain valid.

APPENDIX B

In this appendix, we will develop some of the properties of the G function used in the text, point out two steps for obtaining the boundaries of Chapter II plots, and apply the steps to derive the t_{12} - t_{23} plot boundary for arbitrary masses and overall energy.

The G function is defined by the equation

$$G(a, b; c, d; e, f) = ab(a+b) + cd(c+d) + ef(e+f) + a(cf+de) + b(ce+df)$$

$$-ab(c+d+e+f) - cd(a+b+e+f) - ef(a+b+c+d) . \qquad \text{(B. 1)}$$

This function is invariant under certain permutations of its six variables. For example, $a \leftrightarrow b$, $c \rightarrow e \rightarrow d \rightarrow f \rightarrow c$ leaves G unchanged as does $a \rightarrow c \rightarrow e \rightarrow a$, $b \rightarrow d \rightarrow f \rightarrow b$. All possible products generated by these two operations comprise a group of order twenty four. This group is the symmetry group of the regular octahedron having only even permutations. It consists of (see figure 12):

(1) rotations about the 3-fold symmetry axes perpendicular to the faces of the octahedron;

(2) rotations about the 4-fold symmetry axes passing through two opposite vertices followed by a reflection through the plane containing the other four vertices;

(3) rotations about the 2-fold symmetry axes in the plane of four vertices followed by a reflection through this plane.

The transformations of (1), (2), and (3) correspond to eight, nine, and six operations respectively. These twenty three operations along with the identity form the group.

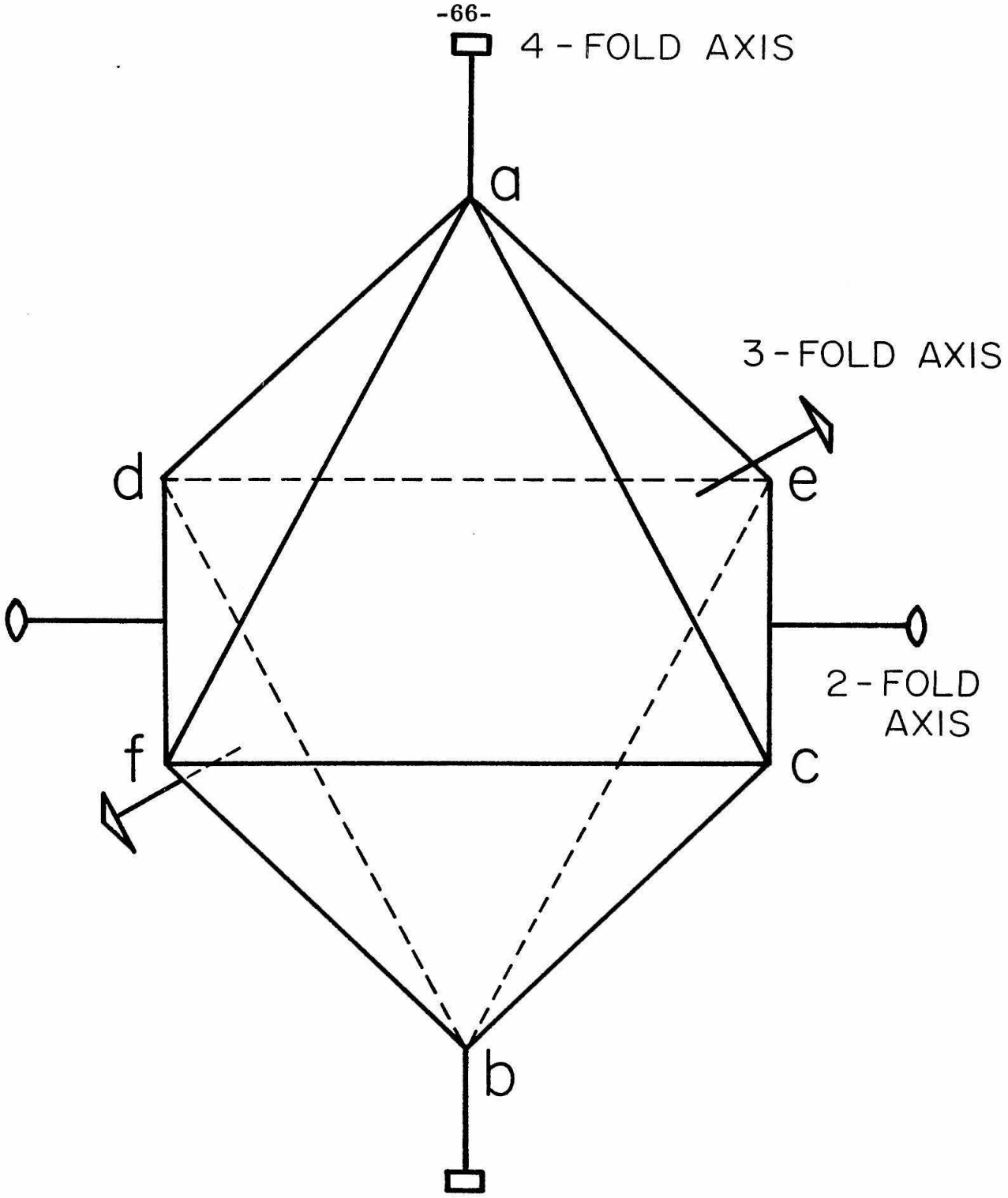

Figure 12. Association of the six arguments of the G-function with the vertices of a regular octahedron with symmetry axes as indicated.

The relationship of the G function to the boundary of the Chew-Low plot is given by Eq. (II. 10) as we shall now demonstrate. Boundaries of the Dalitz and other plots described by the vanishing of the G function are treated similarly. Continuing from Eq. (II. 9), we see that keeping the angle between $\hat{q}_3$ and $\hat{q}_a$ physical requires $(q_3 q_a)^2 - (\vec{q}_3 \cdot \vec{q}_a)^2 \geq 0$, where these vectors are described in the $\vec{q}_b = 0$ frame. In this frame

$$s = (q_a + q_b)^2 = m_a^2 + m_b^2 + 2E_a m_b$$

$$t_{23} = (q_3 - q_b)^2 = m_3^2 + m_b^2 - 2E_3 m_b$$

$$s_{12} = (q_a + q_b - q_3)^2 = m_a^2 + m_b^2 + m_3^2 + 2m_b(E_a - E_3) - 2E_a E_3 + 2\vec{q}_3 \cdot \vec{q}_a . \qquad \text{(B. 2)}$$

Thus, we have

$$4[(\vec{q}_3 \cdot \vec{q}_a)^2 - (q_3 q_a)^2] = \{[s_{12} - s + m_b^2 - t_{23} + 2E_3 E_a]^2 - 4(E_3^2 - m_3^2)(E_a^2 - m_a^2)\}$$

$$= (s_{12} + m_b^2 - s - t_{23})^2 + (s_{12} + m_b^2 - s - t_{23})(m_3^2 + m_b^2 - t_{23})(s - m_a^2 - m_b^2)/m_b^2$$

$$+ m_3^2 (s - m_a^2 - m_b^2)^2/m_b^2 + m_a^2 (m_3^2 + m_b^2 - t_{23})^2/m_b^2 - 4m_a^2 m_3^2$$

$$= \frac{1}{m_b^2}\{t_{23} s(s + t_{23}) + s_{12} m_b^2 (s_{12} + m_b^2) + m_3^2 m_a^2 (m_3^2 + m_a^2)$$

$$+ t_{23}(s_{12} m_a^2 + m_b^2 m_3^2) + s(s_{12} m_3^2 + m_b^2 m_a^2) - s t_{23}(s_{12} + m_b^2 + m_3^2 + m_a^2)$$

$$- s_{12}m_b^2(t_{23}+s+m_3^2+m_a^2) - m_3^2 m_a^2 (t_{23}+s+s_{12}+m_b^2)\}$$

$$= \frac{1}{m_b^2} G(t_{23}, s;\ s_{12}, m_b^2;\ m_3^2,\ m_a^2) \qquad \text{(B. 3)}$$

as stated in Eq. (II. 10). To obtain the Chew-Low plot boundary, we set $G = 0$ and solve this quadratic equation for t_{23}:

$$t_{23} = m_3^2+m_b^2 - \frac{(s+m_b^2-m_a^2)(s+m_3^2-s_{12})}{2s} \pm \frac{\sqrt{\lambda}(s, m_a^2, m_b^2)\lambda(s, m_3^2, s_{12})}{2s}. \qquad \text{(B. 4)}$$

This result was predictable and could have been written down by inspection. For a quasi- two body reaction with initial particles of mass m_a and m_b, final particles of mass $\sqrt{s_{12}}$ and m_3, the momentum exchange t_{23} in the center of mass is

$$t_{23} = (q_3 - q_b)^2 = m_3^2 + m_b^2 - 2E_3E_b + 2q_3q_b \cos\theta$$

$$= m_3^2+m_b^2 - \frac{(s+m_b^2-m_a^2)(s+m_3^2-s_{12})}{2s} + \frac{\sqrt{\lambda}(s, m_a^2, m_b^2)\lambda(s, m_3^2, s_{12})}{2s}$$

$$\times \cos\theta. \qquad \text{(B. 5)}$$

When $\cos\theta = \pm 1$ we obtain the plot boundary given in Eq. (B. 4). Unfortunately, the solution for s_{12} is not so easily written down. We know, however, that the G function is invariant under certain operations, so the solutions to $G = 0$ will be also. In particular, the Chew-Low G is invariant under $s_{12} \leftrightarrow t_{23}$, $s \leftrightarrow m_b^2$, so Eq. (B. 4)

must be also, and without any algebraic work we have

$$s_{12} = s+m_3^2 - \frac{(s+m_b^2-m_a^2)(m_b^2+m_3^2-t_{23})}{2m_b^2} \pm \frac{\sqrt{\lambda}(s, m_b^2, m_a^2)\lambda(m_b^2, m_3^2, t_{23})}{2m_b^2}. \tag{B. 6}$$

Using these two techniques, namely, (1) expressing the process as a quasi- two body reaction and solving for a convenient "momentum transfer", and (2) replacing the "momentum transfer" by the desired variable according to a symmetry of the G function, we can, almost by inspection, construct algebraic solutions for the boundaries of the Chapter II plots.

Consider now the Dalitz plot. A suitable quasi- two body reaction is shown in figure 13. The "momentum exchange" is $s_{12} = (P - q_3)^2 = (q_1 + q_2)^2$, so the boundary solution is

$$s_{12} = s + m_3^2 - 2E_P E_3 \pm 2Pq_3$$

$$= s+m_3^2 + \frac{(s_{23}+s-m_1^2)(s_{23}+m_3^2-m_2^2)}{2s_{23}} \pm \frac{\sqrt{\lambda}(s, s_{23}, m_1^2)\lambda(s_{23}, m_3^2, m_2^2)}{2s_{23}}. \tag{B. 7}$$

In this case, the second step is unnecessary since we could solve for s_{23} as easily as for s_{12}. To illustrate it, nevertheless, we notice that the interchange $s_{12} \leftrightarrow s_{23}$, $m_1^2 \leftrightarrow m_3^2$ gives the solution for s_{23}.

Finally, for the $t_{12} - t_{23}$ plot, we must consider the two suitable quasi- two body reactions shown in figures 14 and 15.

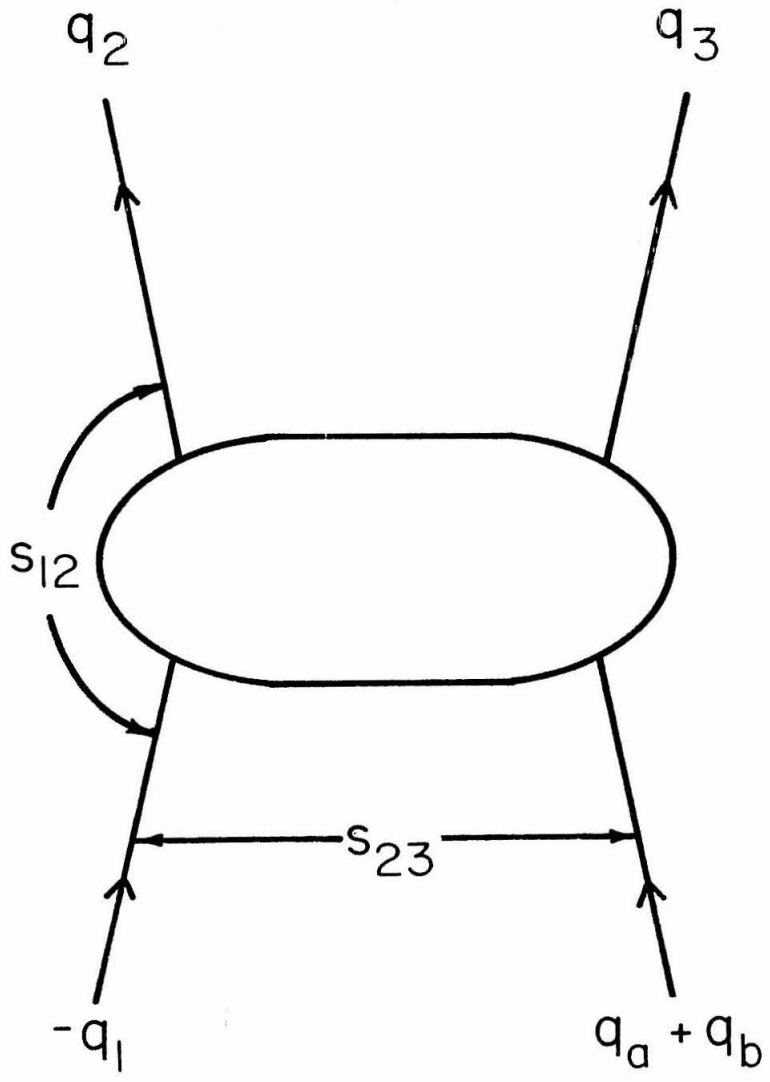

Figure 13. Convenient diagram for obtaining Dalitz plot boundaries.

Solving for the momentum transfers in the center of mass gives in figures 14 and 15 respectively

$$t_{23} = m_a^2+s_{12} - \frac{(s+s_{12}-m_3^2)(s+m_a^2-m_3^2)}{2s} \pm \frac{\sqrt{\lambda}(s, m_a^2, m_b^2)\lambda(s, s_{12}, m_3^2)}{2s} \qquad \text{(B. 8(a))}$$

$$t_{12} = m_1^2+m_a^2 - \frac{(s_{12}+m_1^2-m_2^2)(s_{12}+m_a^2-t_{23})}{2s_{12}} \pm \frac{\sqrt{\lambda}(s_{12},m_1^2,m_2^2)\lambda(s_{12},m_a^2,t_{23})}{2s_{12}} \qquad \text{(B. 8(b))}$$

where $s_{12} = (q_1 + q_2)^2$, $t_{23} = (q_b - q_3)^2$. In (B. 8(a)) we use the transformation $t_{23} \to s_{12} \to m_3^2 \to t_{23}$, $s \to m_b^2 \to m_a^2 \to s$; in (B. 8(b)) we use the transformation $t_{12} \leftrightarrow s_{12}$, $m_2^2 \leftrightarrow m_a^2$. Then we obtain

$$a_\pm(t_{23}) \equiv s_{12} = s+m_3^2 - \frac{(m_b^2+m_3^2-t_{23})(m_b^2+s-m_a^2)}{2m_b^2} \pm \frac{\sqrt{\lambda}(m_b^2, m_3^2, t_{23})\lambda(m_b^2, m_a^2, s)}{2m_b^2} \qquad \text{(B. 9(a))}$$

$$b_\pm(t_{12}, t_{23}) \equiv s_{12} = m_1^2+m_2^2 - \frac{(t_{12}+m_1^2-m_a^2)(t_{12}+m_2^2-t_{23})}{2t_{12}} \pm \frac{\sqrt{\lambda}(t_{12}, m_1^2, m_a^2)\lambda(t_{12}, t_{23}, m_2^2)}{2t_{12}} . \qquad \text{(B. 9(b))}$$

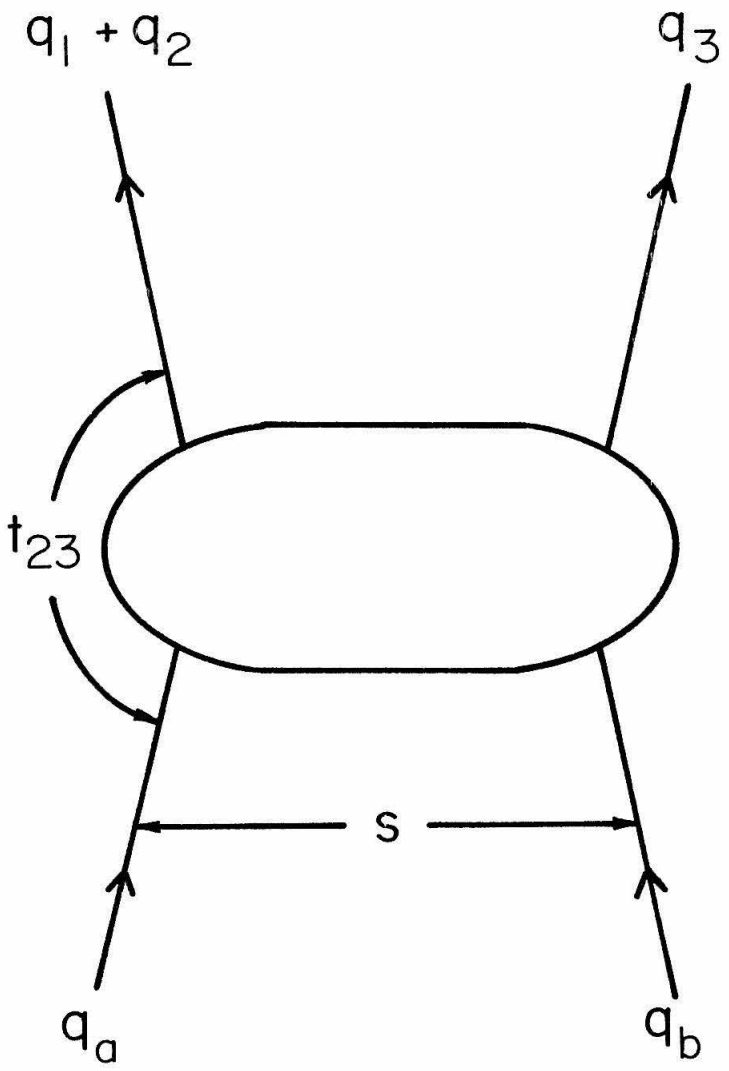

Figure 14. Convenient diagram used in calculating t_{12} - t_{23} plot boundaries.

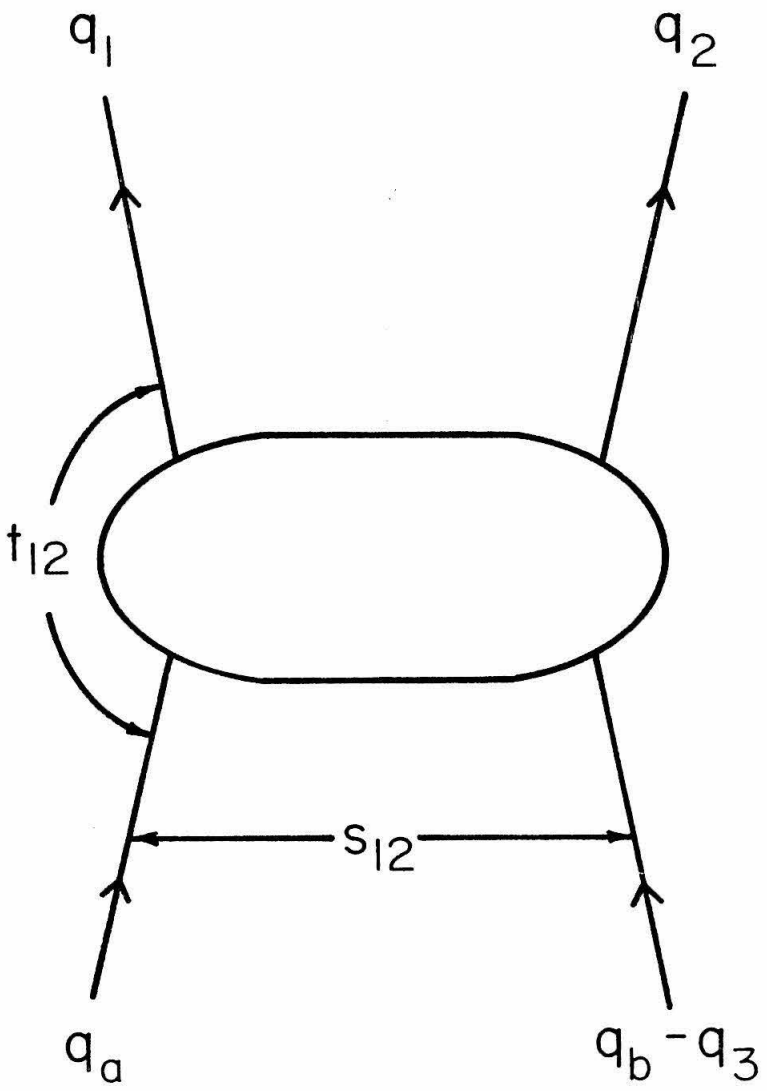

Figure 15. Convenient diagram used in calculating t_{12} - t_{23} plot boundaries.

Notice that Eqs. (B. 9) are the same as Eqs. (II. 18), so we use the same notation $a_{\pm}(t_{23})$, $b_{\pm}(t_{12}, t_{23})$ for the corresponding solutions for s_{12}.

We will develop the t_{12} - t_{23} boundary as a function of t_{23}. First, assume $t_{12} < 0$. Then, s_{12} in the physical region must satisfy $a_- \leq s_{12} \leq a_+$ and $b_+ < b_- \leq s_{12}$. There are two cases to consider:

1. $b_- \geq a_-$. The boundary is given by $b_-(t_{12}, t_{23}) = a_+(t_{23})$
2. $b_- \leq a_-$. The boundary is given by $a_-(t_{23}) = a_+(t_{23})$.

Notice that for the case 2 boundary we have $\sqrt{\lambda}(t_{23}, m_3^2, m_b^2) = 0$, or $t_{23} = (m_3 - m_b)^2$. It is clear from (B. 9(a)) that t_{23} reaches this value in the physical region if, and only if,

$$s + m_3^2 - \frac{m_3(m_b^2 + s - m_a^2)}{m_b} \geq (m_1 + m_2)^2$$

$$\text{or} \quad s \geq m_3 m_b + \frac{m_b(m_1 + m_2)^2 - m_3 m_a^2}{m_b - m_3} \quad . \tag{B. 10}$$

Now, assume $t_{12} > 0$. s_{12} must satisfy $b_- \leq s_{12} \leq b_+$ and $a_- \leq s_{12} \leq a_+$. There are four cases to consider:

1. $a_+ \leq b_+$, $a_- \leq b_-$. The boundary is given by
$$b_-(t_{12}, t_{23}) = a_+(t_{23})$$
2. $a_+ \geq b_+$, $a_- \leq b_-$. The boundary is given by
$b_+(t_{12}, t_{23}) = b_-(t_{12}, t_{23})$, or $t_{12} = (\sqrt{t_{23}} - m_2)^2, t_{23} > 0$

3. $a_+ \geq b_+$, $a_- \geq b_-$. The boundary is given by

$$a_-(t_{23}) = b_+(t_{12}, t_{23}).$$

4. $a_+ \leq b_+$, $a_- \geq b_-$. The boundary is given by

$$a_+(t_{23}) = a_-(t_{23}) \text{ or } t_{23} = (m_3 - m_b)^2 .$$

When $a_\pm(t_{23}) = b_\pm(t_{12}, t_{23})$, we can solve for t_{12} in terms of t_{23} by using expression (B. 8(b)) and substituting in $a_\pm(t_{23})$ from (B. 9(a)). We will then obtain four values of t_{12} for each value of t_{23} corresponding to the four branches. We then use the above rules to decide which branches are physical. We immediately have that if $a_-(t_{23})$ is used, the resulting branch with $t_{12} < 0$ is not physical. Also, the condition $t_{12} < (m_1 - m_a)^2$ eliminates non-physical branches. For the remaining branches, we must check the inequalities given in the above rules for $a_\pm(t_{23})$, $b_\pm(t_{12}, t_{23})$ to decide the final $t_{12} - t_{23}$ boundary.

APPENDIX C

In this appendix we will derive the multi-Regge amplitude for particles with spin. This amplitude is required for the discussion of decay distributions of final state resonances in reactions that may receive large multi-Regge contributions. For such decay distributions, the spinless theory of Chapter III is inadequate, as is the work of references (3), (4), and (5) in which spin is neglected or crossing is not treated.

We turn now to the problem of stating the N body crossing relations. For two body processes, Trueman and Wick[33], and, more recently, Cohen-Tannondji, et. al.[34] have given the crossing relations for helicity amplitudes. Capella[35] generalizes the results of reference (34) to processes with N final particles. This generalization requires certain plausible assumptions concerning analytic continuation of cross channel amplitudes back to the direct channel which, as yet, have been proven only for two body final states[36]. Following Capella we consider the process (see figure 6).

$$a + b \rightarrow 1 + 2 + \cdots + N \qquad (C.1)$$

with s_i, λ_i $(i = a, b, 1, \ldots, N)$ being the spins and center of mass helicities of the particles, and $G_{\lambda_1 \cdots \lambda_N ; \lambda_a \lambda_b}$ being the helicity amplitude for this channel, hereafter referred to as the direct channel. Notice that in the center of mass of this channel, the helicity λ_i is the spin projection of particle i in its rest frame

along the direction $-(\vec{q}_a + \vec{q}_b)$, or covariantly, along the direction $-m_i^2(q_a + q_b) + (q_a + q_b) \cdot q_i \, q_i$. Furthermore, let $F_{\mu_b \mu_2 \cdots \mu_N; \mu_a \mu_1}$ be the corresponding helicity amplitude for the crossed process

$$a + \bar{1} \to \bar{b} + 2 + \cdots + N \qquad (C.2)$$

where the helicity μ_i is the spin projection of particle i along the direction $-m_i^2(q_a + q_{\bar{1}}) + (q_a + q_{\bar{1}}) \cdot q_i q_i$. Capella, then, derives the crossing relation

$$G_{\lambda_1 \cdots \lambda_N; \lambda_a \lambda_b} = e^{-i\pi(\lambda_a + \lambda_2 + \cdots + \lambda_N)} \sum_{\mu_1 \cdots \mu_N \mu_a \mu_b} d^{s_a}_{\mu_a \lambda_a}(\chi_a) \, d^{s_b}_{\mu_b \lambda_b}(\chi_b)$$

$$\times \, d^{s_1}_{\mu_1 \lambda_1}(\chi_1) \cdots d^{s_N}_{\mu_N \lambda_N}(\chi_N) \, F^c_{\mu_b \mu_2 \cdots \mu_N; \mu_a \mu_1} \qquad (C.3)$$

where $F^c_{\mu_b \mu_2 \cdots \mu_N; \mu_a \mu_1}$ is the analytic continuation of $F_{\mu_b \mu_2 \cdots \mu_N; \mu_a \mu_1}$ into the direct channel. The $d^{s_i}_{\mu_i \lambda_i}(\chi_i)$ are the rotation matrices whose arguments χ_i are treated presently. For our purposes here we note the following: under crossing $q_i \to q_i$, $i = a, 2, \ldots, N$, $q_{\bar{b}} \to -q_b$, and $q_{\bar{1}} \to -q_1$, so the helicity direction becomes $-m_i^2(q_a - q_1) + (q_a - q_1) \cdot q_i \, q_i$. Thus, in the rest frame of particle i, helicity μ_i is its spin projection along the direction $\vec{q}_1 - \vec{q}_a$. Since $d^{s_i}_{\mu_i \lambda_i}(\chi_i)$ gives the amplitude that its spin projection along $-(\vec{q}_a + \vec{q}_b)$ is λ_i, where χ_i is the angle between $\vec{q}_1 - \vec{q}_a$ and $-(\vec{q}_a + \vec{q}_b)$, we readily see that Eq. (C.3) is exactly what is needed to express $G_{\lambda_1 \cdots \lambda_N; \lambda_a, \lambda_b}$ in terms of $F^c_{\mu_b \mu_2 \cdots \mu_N; \mu_a, \mu_1}$.

From the orthogonality of the rotation matrices we have a form for the cross section analogous to the one for two body reactions, namely,

$$\sigma_N \propto \sum_{\lambda_a\lambda_b\lambda_1\cdots\lambda_N} |G_{\lambda_1\lambda_2\cdots\lambda_N;\,\lambda_a\lambda_b}|^2$$

$$= \sum_{\mu_a\mu_b\mu_1\cdots\mu_N} |F^c_{\mu_b\mu_2\cdots\mu_N;\,\mu_a\mu_1}|^2 \quad . \tag{C.4}$$

Let us assume particle i is a resonance and consider its density matrix. By definition, we have,

$$\bar{\rho}_{\lambda_i,\lambda_i'} = \bar{N} \sum_{\lambda \neq i} G_{\lambda_i;\lambda}\, G^*_{\lambda_i';\lambda} \tag{C.5}$$

where λ means all helicities except λ_i, and $\bar{N} = (TR\ \bar{\rho})^{-1}$. When the density matrix is expressed in terms of the cross channel helicity amplitudes, great simplification occurs if we use the prescription of Gottfried and Jackson[37]. They define

$$\rho_{\mu_i,\mu_i'} = N \sum_{\lambda_i,\lambda_i'} e^{i\varphi_i(\lambda_i-\lambda_i')}\, d^{s_i}_{\mu_i\lambda_i}(\chi_i)\, d^{s_i}_{\mu_i'\lambda_i'}(\chi_i)\, \bar{\rho}_{\lambda_i,\lambda_i'} \tag{C.6}$$

where $N = (TR\ \rho)^{-1}$. The angle χ_i is the same angle used in Eq. (C.3) and φ_i equals π or 0 if particle i is crossed or uncrossed respectively. The indices μ_i, μ_i' are the spin projections of particle i in its rest frame along the direction $\vec{q}_1 - \vec{q}_a$. Combining Eqs. (C.3), (C.5), and (C.6) we have

$$\rho_{\mu_i,\mu_i'} = N \sum_{\lambda \neq i} F^c_{\mu_i;\lambda}\, F^{c\,*}_{\mu_i';\lambda} \quad . \tag{C.7}$$

Now that the cross section and density matrices are defined for the cross channel helicity amplitudes, it remains to express these amplitudes in the multi-Regge form. Using the same variables as in Eq. (III. 6), we find from the work of references (3), (4), and (32) that for fixed $t_{i,i+1}$ and ω_i, as the $s_{i,i+1}$ simultaneously become large, the amplitude assumes the multi-Regge form

$$F^{c}_{\lambda_b\lambda_2\cdots\lambda_N;\lambda_a\lambda_1}(s_{i,i+1}, t_{i,i+1}, \omega_i)\, s_{12}, s_{23}, \ldots, s_{N-1,N} \to \infty \sim$$

$$\beta_{\lambda_a\lambda_1}\, s_{12}^{\alpha_1(t_{12})}\, \zeta_1(t_{12})\, \gamma_{\lambda_2} \cdots \gamma_{\lambda_{N-2}}\, s_{N-1,N}^{\alpha_{N-1}(t_{N-1,N})}\, \zeta_{N-1}(t_{N-1,N}) \times \beta_{\lambda_b\lambda_N}$$

$$\zeta_k(t) = \frac{1 \pm \exp(-i\pi\alpha_k(t))}{\Gamma(1+\alpha_k(t))\, \mathrm{SIN}\pi\, \alpha_k(t)}\,, \quad k = 1, \ldots, N-1 \qquad \text{(C.8)}$$

where, for simplicity of notation, the dependence of the β's and γ's on the relevant trajectories has been suppressed.

Let us now see how the residues $\beta_{\lambda_a\lambda_1}$ and $\beta_{\lambda_b\lambda_1}$ are related to the corresponding two body residues. For $\beta_{\lambda_a\lambda_1}$, in both the N body and two body cases, λ_a and λ_1 represent spin projections of the particles a and 1 in their respective rest frames along $(\vec{q}_1 - \vec{q}_a)$. So, the multi-Regge hypothesis requires

$$\beta_{\lambda_a\lambda_1} = \beta^{(2)}_{\lambda_a\lambda_1}(t = t_{12}) \qquad \text{(C.9)}$$

where $\beta^{(2)}_{\lambda_a\lambda_1}(t)$ is the two body factorized residue that depends only on momentum exchange t. For $\beta_{\lambda_b\lambda_N}$, the situation is not so simple. In the two body residue $\beta^{(2)}_{\lambda_b\lambda_N}(t)$, λ_b and λ_N represent spin

projections of particles b and N in their respective rest frame along $-(\vec{q}_b - \vec{q}_N)$ (since $\vec{q}_a + \vec{q}_b = \vec{q}_1 + \vec{q}_N$ for the two body processes). In the N body residue $\beta_{\lambda_b \lambda_N}$, λ_b and λ_N represent respective rest frame spin projections of particles b and N along $\vec{q}_1 - \vec{q}_a$. If $\mathcal{R}_i (i = b, N)$ is the rotation that carries $-(\vec{q}_b - \vec{q}_N)$ into $\vec{q}_1 - \vec{q}_a$ in the particle i rest frame, then we see that

$$\beta_{\lambda_b \lambda_N} = \sum_{\mu_b \mu_N} \mathcal{D}^{s_b}_{\mu_b \lambda_b}(\mathcal{R}_b)\, \mathcal{D}^{s_N}_{\mu_N \lambda_N}(\mathcal{R}_N)\, \beta^{(2)}_{\mu_b \mu_N}(t = t_{N-1,N}) \qquad (C.10)$$

where the $\mathcal{D}^{s_i}_{\mu_i \lambda_i}(\mathcal{R}_i)$ are the full rotation matrices. In general, the rotations $\mathcal{R}_b$, $\mathcal{R}_N$ will not depend only on $t_{N-1,N}$, so, when spin is present, $\beta_{\lambda_b \lambda_N}$ is not a function of $t_{N-1,N}$ only.

Consider now the internal residue γ_{λ_i}. It is not present in two body interactions, but first appears in three body final states. For the three body case, $\gamma^{(3)}_{\lambda_2} = \gamma^{(3)}_{\lambda_2}(t_{12}, \omega_2, t_{23})$ where λ_2 is the spin projection in the rest frame of particle 2 along $\vec{q}_1 - \vec{q}_a$. Correspondingly, in the N body case, the internal residue $\gamma^{(3)}_{\mu_i}(t_{i-1,i}, \omega_i, t_{i,i+1})$ has spin projection along $(\vec{q}_1 + \ldots + \vec{q}_{i-1} - \vec{q}_a)$. But, in Eq. (C.8) all helicities are referred to the direction $\vec{q}_1 - \vec{q}_a$, so if the rotation $\mathcal{R}_i'$ in the rest frame of particle i carries $(\vec{q}_1 + \ldots + \vec{q}_{i-1} - \vec{q}_a)$ into $\vec{q}_1 - \vec{q}_a$, we see that

$$\gamma_{\lambda_i} = \sum_{\mu_i} \mathcal{D}^{s_i}_{\mu_i \lambda_i}(\mathcal{R}_i')\, \gamma^{(3)}_{\mu_i}(t_{i-1,i}, \omega_i, t_{i,i+1}),\ i = 2, \ldots, N-1 \qquad (C.11)$$

where the γ_{λ_i} are the internal residues appearing in Eq. (C.8).

Since the rotations $\mathcal{R}_i'$ will not, in general, depend only on $t_{i-1,i}$, ω_i, and $t_{i,i+1}$, the residues γ_{λ_i} also will not depend only on them.

We now will derive expressions for the rotations required to align the helicity axes of the cross channel with those of the direct channel. Also, we will give expressions for rotations that align helicity axes of different cross channels continued to the direct channel.

First, let us define for each particle of a reaction in a given channel a tetrad of orthonormal four vectors[34, 35]. Consider the process of Eq. (C. 1). For particle i (i = a, b, 1,..., N), the timelike unit vector is given by $n_0(i) = q_i/m_i$. The helicity axis defines the 3-axis:

$$n_3(i) = -\frac{m_i^2 P - (q_i \cdot P) q_i}{m_i[(q_i \cdot P)^2 - m_i^2 P^2]^{1/2}}, \quad P = q_a + q_b = q_1 + \ldots + q_N. \tag{C. 12}$$

Notice that $[n_3(i)]^2 = -1$ and $n_3(i) \cdot q_i = 0$. In the rest frame of particle i, $n_3(i)$ is parallel to $-(\vec{q}_a + \vec{q}_b)$ which is the usual definition of the center of mass helicity axis. There is no unique way of choosing the z-axis of the tetrad. A convenient choice is

$$n_2^{\mu}(a) = n_2^{\mu}(b) = n_2^{\mu}(1) = \frac{\epsilon^{\mu}{}_{\nu\rho\sigma} q_a^{\nu} q_b^{\rho} q_1^{\sigma}}{[-\epsilon^{\mu}{}_{\nu\rho\sigma} q_a^{\nu} q_b^{\rho} q_1^{\sigma} \epsilon_{\mu\alpha\beta\gamma} q_a^{\alpha} q_b^{\beta} q_1^{\gamma}]^{1/2}}$$

$$n_2^{\mu}(k) = - \frac{\epsilon^{\mu}{}_{\nu\rho\sigma}(q_a{}^{\nu}q_b{}^{\rho}q_k{}^{\sigma} + q_a{}^{\nu}q_1{}^{\rho}q_k{}^{\sigma} + q_b{}^{\nu}q_1{}^{\rho}q_k{}^{\sigma})}{[-\epsilon^{\mu}{}_{\nu\rho\sigma}(q_a{}^{\nu}q_b{}^{\rho}q_k{}^{\sigma}+q_a{}^{\nu}q_1{}^{\rho}q_k{}^{\sigma}+q_b{}^{\nu}q_1{}^{\rho}q_k{}^{\sigma})\epsilon_{\mu\alpha\beta\gamma}(q_a{}^{\alpha}q_b{}^{\beta}q_k{}^{\gamma}+q_a{}^{\alpha}q_1{}^{\beta}q_k{}^{\gamma}+q_b{}^{\alpha}q_1{}^{\beta}q_k{}^{\gamma})]^{1/2}}$$

$$, \quad k = 2, \ldots, N . \qquad \text{(C.13)}$$

For two body processes (C.13) reduces to $n_2{}^{\mu}(a) = n_2{}^{\mu}(b) = n_2{}^{\mu}(1) = n_2{}^{\mu}(2) \propto \epsilon^{\mu}{}_{\nu\rho\sigma}\, q_a{}^{\nu}q_b{}^{\rho}q_1{}^{\sigma}$ which is the normal to the production plane. The 1-axis is defined from the 2- and 3-axes by the right hand rule

$$n^{\mu}{}_1(i) = \epsilon^{\mu}{}_{\nu\rho\sigma}\, n_0{}^{\nu}(i)\, n_2{}^{\rho}(i)\, n_3{}^{\sigma}(i) \ . \qquad \text{(C.14)}$$

In these definitions the final particles do not play symmetric roles, but rather, particle 1 is singled out. The definitions are most convenient for describing processes in which particle 1 is one of the crossed particles. Therefore, we consider the crossed process of (C.2) with q_i' ($i = a, \bar{b}, \bar{1}, 2, \ldots N$) denoting the momenta. The tetrads for this channel are

$$n_0'(i) = q_i'/m_i$$

$$n_3'(i) \propto -m_i^2\, P' + (P' \cdot q_i')q_i', \quad P' = q_1' + q_a'$$

$$n_2'(a) = n_2'(b) = n_2'(1) \propto \epsilon^{\mu}{}_{\nu\rho\sigma}\, q_a'{}^{\nu}\, q_1'{}^{\rho}\, q_b'{}^{\sigma}$$

$$n_2'(k) \propto -\epsilon^{\mu}{}_{\nu\rho\sigma}(q_a'^{\nu} q_1'^{\rho} q_k'^{\sigma} + q_a'^{\nu} q_b'^{\rho} q_k'^{\sigma} + q_1'^{\nu} q_b'^{\rho} q_k'^{\sigma})$$

$$, \; k = 2, \ldots, N . \qquad \text{(C.15)}$$

When these crossed channel tetrads are continued back to the direct channel, they become $\{\pm q_i/m_i,\ n'_1{}^{c}(i),\ n'_2{}^{c}(i) = -n_2(i),\ n'_3{}^{c}(i)\}$ where the - or + sign holds for crossed or uncrossed particles respectively. The continuation requires $q'_i = q_i$, $i = a, 2, \ldots, N$, and $q'_i = -q_i$, $i = 1, b$. For example,

$$n'_3{}^{c}(i) = \frac{-m_i^2(q_a - q_1) + [(q_a - q_1)\cdot q_i]q_i}{m_i\{[(q_a - q_1)\cdot q_i]^2 - m_i^2(q_a - q_1)^2\}^{1/2}} . \qquad \text{(C.16)}$$

The continued tetrads are related to the direct channel tetrads by a product of rotations. For the uncrossed particles, the product is a rotation through angle χ_i about the 2-axis followed by a rotation through π about the 3-axis where

$$\text{COS}\,\chi_i = -n'_3{}^{c}(i) \cdot n_3(i)$$

$$\text{SIN}\,\chi_i = -n'_1{}^{c}(i) \cdot n_3(i) , \quad i = a, 2, \ldots, N . \qquad \text{(C.17)}$$

These χ_i are the arguments of the rotation matrices of Eq. (C. 3). (It turns out (C.17) gives the angles for the crossed particles b and 1 also as shown in references (34) and (35)). More explicitly, in terms of the invariants we have

$$\text{COS}\,\chi_i = \frac{(q_a - q_1)\cdot q_i\,(q_a + q_b)\cdot q_i - m_i^2(q_a - q_1)\cdot(q_a + q_b)}{\{[(q_a - q_i)\cdot q_i]^2 - m_i^2(q_a - q_1)^2\}^{1/2}\{[(q_a+q_b)\cdot q_i]^2 - m_i^2(q_a+q_b)^2\}^{1/2}} \tag{C.18}$$

Now consider the reaction

$$\bar{N} + b \rightarrow 1 + 2 + \cdots + (N-1) + \bar{a} \ . \tag{C.19}$$

In this channel the tetrads are

$$m'_0(i) = q'_i / m_i$$

$$m'_3(i) \propto -m_i^2\,(q'_b + q'_N) + (q'_b + q'_N)\cdot q_i\, q_i$$

$$m'_2(a) = m_i(b) = m'_2(N) \propto \epsilon^{\mu}{}_{\nu\rho\sigma}\, q'_b{}^{\nu}\, q'_N{}^{\rho}\, q'_a{}^{\sigma}$$

$$m'_2(k) \propto -\epsilon^{\mu}{}_{\nu\rho\sigma}(q'_b{}^{\nu} q'_N{}^{\rho} q'_k{}^{\sigma} + q'_b{}^{\nu} q_a'^{\rho} q_k'^{\sigma} + q'_N{}^{\nu} q_a'^{\rho} q'_k{}^{\sigma}),$$

$$k = 1, \ldots, N-1 \ . \tag{C.20}$$

When continued back to the direct channel ($q'_i \rightarrow q_i$, $i = b, 1, \ldots, N-1$; $q'_i \rightarrow -q_i$, $i = a, N$), these tetrads differ from the continuation of (C.15) by a product of rotations. Let α_i, β_i, γ_i be the Euler angles of the rotations that take the triads $\{n'^c_1(i),\ n'^c_2(i),\ n'^c_3(i)\}$ into the triads $\{m'^c_1(i),\ m'^c_2(i),\ m'^c_3(i)\}$. Then,

$$\text{COS}\,\gamma_i\,\text{SIN}\,\beta_i = -n'^c_3(i)\cdot m'^c_1(i)$$

$$\text{COS}\,\alpha_i\,\text{SIN}\,\beta_i = -n'^c_1(i)\cdot m'^c_3(i)$$

$$\cos \beta_i = -n_3^{'c}(i) \cdot m_3^{'c}(i) \ . \qquad \text{(C. 21)}$$

These results define the rotations $\mathcal{R}_b$ and $\mathcal{R}_N$ of Eq. (C. 10) which are involved in transforming the external vertices.

The rotations of Eq. (C. 11) needed to transform the internal vertices are calculated analogously.

II. High Energy Model for Proton-Proton Scattering

CHAPTER I

Introduction

Several years ago, Wu and Yang[1] suggested that the pp scattering cross section at large momentum transfers should be proportional in its t dependence to the fourth power of the proton charge form factor. The basis of their argument was the idea that the proton could be regarded as an extended system with a structure which is reflected in elastic electron-proton scattering. The rapid decrease in the values of the pp elastic-scattering cross section and the proton form factors away from $t = 0$ results, in this view, from the breakup of this extended structure when the momentum transfer between the particles is large. These ideas were developed further by Byers and Yang[2] in their discussion of small-angle diffraction scattering (coherent droplet model). More recently, Chou and Yang[3] have used the droplet model and information on pp and πp scattering to predict the t dependence of the charge form factor of the pion.

In Chapter II we define the model and, from it, derive the formulae for the scattering amplitude and for the S-matrix at a given impact parameter. The high momentum transfer limit of the scattering amplitude is found to be proportional to the product of the form factors of elastically scattering hadrons. In Chapter III we present the results of cross section calculations for a purely absorptive model and for one with a small amount of refraction of the incident wave. We consider possible spin dependence using a weak spin-orbit type interaction to predict pp polarization. In Chapter IV our conclusions

and predictions concerning the asymptotic limit of hadron-hadron scattering are stated, along with some brief comments on further experimental tests.

CHAPTER II

Definition of the Model

We wish to discuss high-energy pp scattering on the basis of the Byers-Chou-Wu-Yang model. The physical assumptions which underlie the model can be summarized as follows: (i) The elastic scattering of hadrons at high energies is primarily diffractive, resulting from the absorption of the incident wave into the many open inelastic channels (breakup of the extended structure). (ii) At sufficiently high energies, the absorption occurs locally, and is proportional, for any impact parameter, to the total amount of inter-penetrating hadronic matter. The S-matrix element for the elastic scattering of hadrons A and B at an impact parameter b can then be expressed as an integral over the matter distributions,[2,3] or more conveniently, as

$$S(b) = \exp\{-\varkappa\rho(b)\} \quad , \tag{II. 1}$$

where $\varkappa$ is an absorption coefficient, possibly complex and energy dependent, and $\rho(b)$ is the weight function in the Fourier-Bessel representation of the product of the hadronic matter form factors,

$$G_A(t)G_B(t) = \int_0^\infty \rho(b)J_0(b\sqrt{-t})\, bdb \, . \tag{II. 2}$$

The eikonal type approximation used in the derivation of this result requires the momentum in the center of mass to be large compared with the greater of μ and $\sqrt{-t}$, where μ is the reciprocal

of the characteristic size of the colliding particles. Spin dependence of the absorption has been neglected in deriving this result, but will be considered presently.

It is clear from the derivation of Eq. (II. 1) from an integral over the hadronic matter densities, assumed always to be positive, that $\rho(b)$ is positive for all b, and hence that $|S(b)| < 1$ if $\mathrm{Re}\,\varkappa > 0$. The weight function $\rho(b)$ can be expressed in terms of the spectral weights $\sigma(t')$ in the dispersion relations for the matter form factors:

$$G(t) = \int_{t_0}^{\infty} \sigma(t')\,(t' - t)^{-1}\,dt' ,$$

$$\rho(b) = \int_{t_A}^{\infty} dt' \int_{t_B}^{\infty} dt''\,\sigma_A(t')\,\sigma_B(t'')$$

$$\times\,[K_0(b\sqrt{t'}) - K_0(b\sqrt{t''})]\,(t'' - t')^{-1} . \qquad \text{(II. 3)}$$

The scattering amplitude is given by the familiar integral over impact parameters,

$$f(s, t) = i \int_0^{\infty} [1 - S(b)]\,J_0(b\sqrt{-t})\,b\,db . \qquad \text{(II. 4)}$$

The normalization of $f(s, t)$ is such that the differential elastic-scattering cross section and the total cross section are given by

$$d\sigma/dt = \pi |f(s, t)|^2 , \qquad \text{(II. 5)}$$

$$\sigma_T = 4\pi\,\mathrm{Im}\,f(s, 0) . \qquad \text{(II. 6)}$$

The asymptotic form of the scattering amplitude for $-t \to \infty$ is easily derived using the general expression for $\rho(b)$ given in Eq. (II. 3). Provided the spectral weights $\sigma(t')$ decrease rapidly for $t' \to \infty$,

$$f(s,t) \underset{t \to -\infty}{\longrightarrow} i\varkappa e^{-\varkappa\rho(0)} \times G_A(t)G_B(t)[1 + O(\mu^2/t)] , \qquad \text{(II. 7)}$$

where μ^2 is the characteristic value of t'. To the extent that the distribution of hadronic matter in the proton is similar to the distribution of charge, the product of matter form factors in Eq. (II. 7) can be approximated for pp scattering by the square of the proton charge form factor, $G_p^2 \to G_E^2$. This approximation yields a Wu-Yang-type[1] model for pp scattering at large momentum transfers, but with a constant of proportionality between $f(s,t)$ and G_E^2 which is determined by the absorption constant $\varkappa$, hence, indirectly, by the pp total cross section.

We remark finally that $\mathrm{Im}f(s,t)$ is positive for pp scattering for $t \to 0$ and $t \to -\infty$, and can consequently have at most an even number of diffraction zeros in the interval $0 \geq t$.

We have applied the foregoing model to high-energy pp scattering using as input the empirical fit to the measured proton form factor,[4]

$$G_p(t) \sim G_E(t) \sim [\mu^2/(\mu^2 - t)]^2 ,$$

$$\mu = 0.71 \ (\mathrm{GeV}/c)^2 . \qquad \text{(II. 8)}$$

In this case, S(b) is given by

$$S(b) = \exp\{-\frac{1}{8} A(\mu b)^3 K_3(\mu b)\} , \qquad \text{(II. 9)}$$

where K(x) is the hyperbolic Bessel function of the second kind. The absorption constant has been redefined in Eq. (II. 9) so that $S(0) = e^{-A}$.

CHAPTER III

Calculations and Results

Scattering cross sections were calculated for a number of values of μ^2 close to that quoted in Eq. (II. 8). We found it convenient for numerical calculations to evaluate f(s, t) using a partial-wave series which is equivalent to the impact-parameter integral in Eq. (II. 4) for small scattering angles and high energies. The requisite partial-wave S-matrix elements are given by

$$S_j = \exp\{A(z-1)^3 Q_j^{(3)}(z)\}, \quad z = 1 + \mu^2/2p^2 . \qquad \text{(III. 10)}$$

where $Q_j^{(3)}(z)$ is the third derivative of the Legendre function of the second kind. The real part of the parameter A was determined by fitting the asymptotic pp total cross section, taken as 35. 7 mb.[5] In those cases in which A was chosen complex, corresponding to refraction as well as absorption of the incident wave in the scattering, ImA was determined by fitting the real part of the forward pp scattering amplitude measured at 26 GeV/c[6]; ImA must decrease slowly with increasing energy. Finally, the effects of a possible spin dependence of the absorption were investigated by adding to f(s, t) a term corresponding to a weak spin-orbit-type interaction,

$$f_{LS}(s,t) = i(\vec{\sigma}_1 + \vec{\sigma}_2) \cdot \hat{n} \times \int_0^\infty S(b)\varkappa'\rho'(b) J_1(b\sqrt{-t})\, b\, db . \qquad \text{(III. 11)}$$

Satisfactory fits to the pp polarization observed in references (7) and (8) were obtained using the distribution

$$\varkappa'\rho'(b) \rightarrow C(\mu b)^4 K_3(\mu b) . \qquad \text{(III. 12)}$$

A more natural choice for $\rho'(b)$ would involve the function $(\mu b)^3 K_2(\mu b)$. The spin-dependent and spin-independent interactions would then be related in the manner familiar for spin-orbit couplings in potential scattering. However, the resulting polarization would be proportional to $\sqrt{-t}$ over too wide a range of t to be consistent with present data (see references (7) and (8)). The choice for $\rho'(b)$ given in Eq. (III. 12) corresponds to a more diffuse spatial distribution of the spin-dependent term. The details of the polarization predicted in Fig. 2 depend on the choice of $\rho'(b)$. The existence of structure of the type shown does not, provided the existing data are fitted.

The results of the present calculations are quite striking (Figs. 1 and 2). Curve a in Fig. 1 gives the asymptotic pp cross section calculated for $\mu^2 = 1.0\ (\text{GeV/c})^2$. For smaller values of μ^2, the diffraction zeroes move closer together and eventually merge and disappear for $\mu^2 \sim 0.6\ (\text{GeV/c})^2$. The predicted cross section is unreasonably small for $-t \sim 2\text{-}4\ (\text{GeV/c})^2$ for the value of μ^2 quoted in reference (4): $\mu^2 = 0.71\ (\text{GeV/c})^2$. Within the uncertainty of the model, the larger values of μ^2 necessary to obtain a reasonable cross section in this region indicate that the matter distribution of the proton is about 15% more compact than the charge distribution. It should be emphasized that we have not attempted to find a best fit to the data now available, e. g., by using a more flexible form for G_p. The cross section displays two diffraction

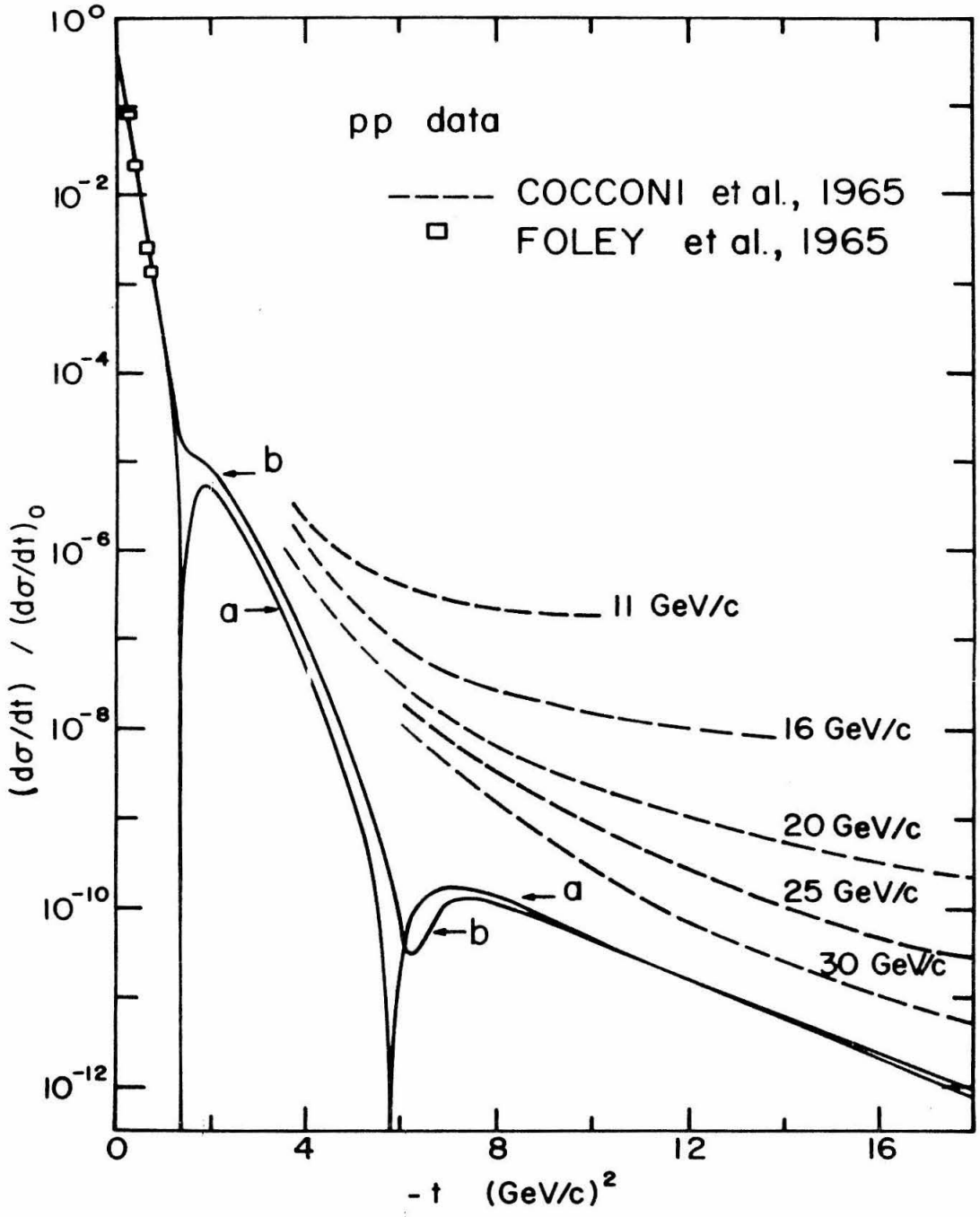

Figure 1 . Comparison of predicted asymptotic pp-scattering cross section with present experimental data. Curve a, prediction for case of pure absorption, μ^2, = 1.0 $(GeV/c)^2$, A = 1.64. Curve b, prediction including real part, μ^2 = 1.0 $(GeV/c)^2$, ReA = 1.62, ImA = 0.34. Experimental data from Foley et al. and Cocconi et al., reference (10).

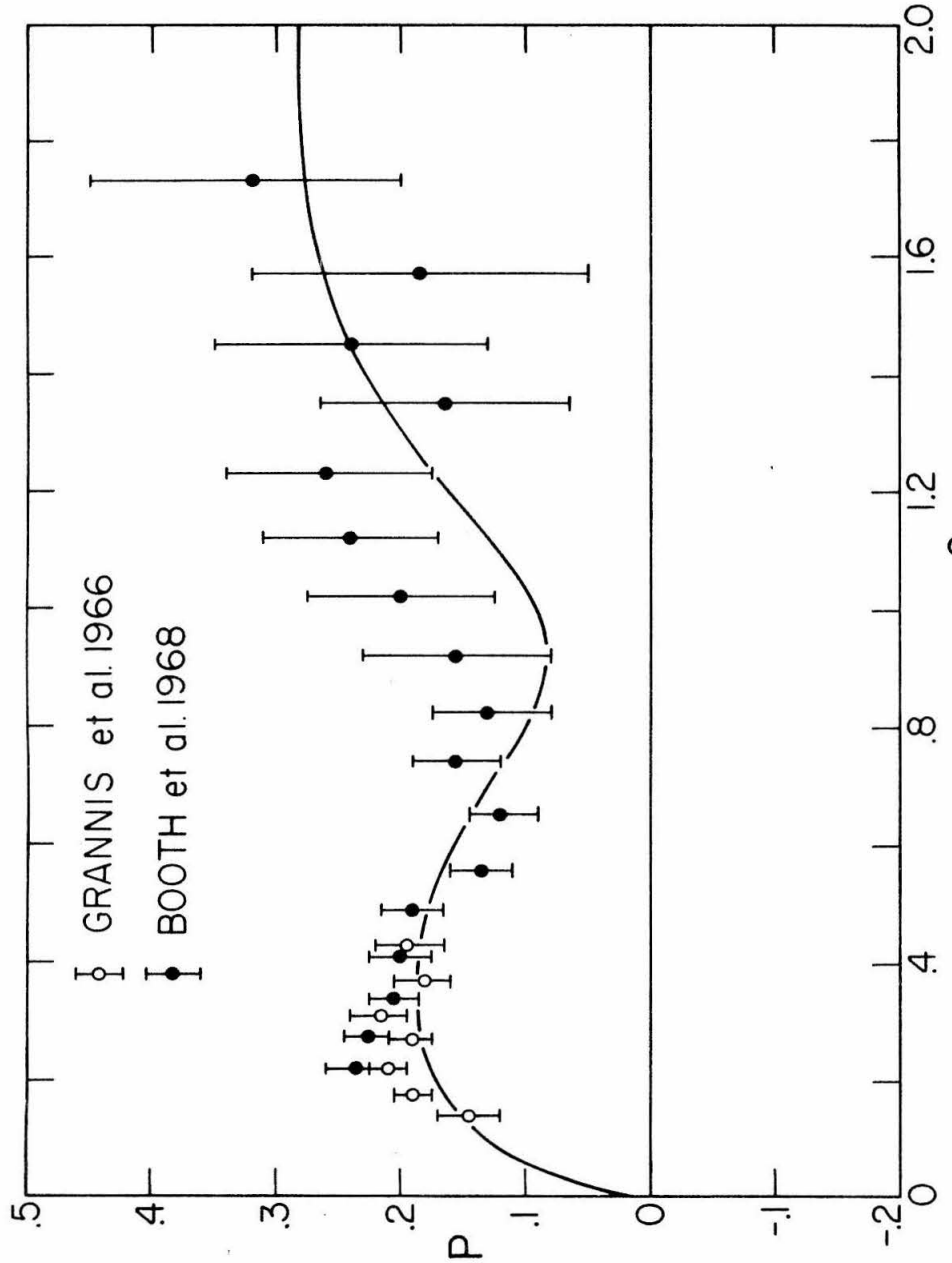

Figure 2. Predictions for pp polarization at 5 BeV/c with C = .031. Experimental data from Booth et al. at 5.15 BeV/c, reference (8), and Grannis et al. at 4.84 BeV/c, reference (7).

zeros which are partially filled in when the real part of the scattering amplitude is included, curve b. The structure is further washed out by the spin-dependent contributions to the cross section. The result is a "break" or "dip" structure in $d\sigma/dt$ reminiscent of that observed by Akerlof et al. and by Allaby et al.[9]

It should be emphasized that the diffraction zeros result from a typical interference effect which involves both protons, and do not reflect any distinctive structure in the individual matter distributions.

It is evident in Fig. 1 that the experimental pp scattering cross sections[10] at the highest energies now available agree quite well with the theoretical cross sections for $-t \lesssim 1$ $(GeV/c)^2$. The rapid shrinkage of the experimental cross sections for large values of $-t$ is also consistent with the asymptotic nature of the model: The model should give the high-energy limit of $d\sigma/dt$. The experimental cross sections at fixed s should be less nearly asymptotic the larger the value of $-t$.

CHAPTER IV

Conclusions and Predictions

The major results predicted by the present model can be summarized as follows:

(1) At high energies and fixed momentum transfers, hadron-hadron scattering cross sections should approach an asymptotic limit given by the diffraction model. This limit may be ascribed in different language to the non-shrinking asymptotic contributions of the Pomeranchuk Regge trajectory and its associated cuts.[11] Those contributions which disappear with increasing s should be describable by other Regge exchanges (P', ω, ρ, etc.).

(2) The asymptotic pp scattering cross section should display two diffraction minima. The minima should appear in experiments at high, but nonasymptotic, energies, and become increasingly prominent with increasing energy as the real part of the scattering amplitude and the spin-dependent terms decrease in importance. The exact positions of the minima are model dependent, but appear most likely to lie in the ranges $-t = 1\text{-}2$ $(\text{GeV}/c)^2$ and $-t = 5\text{-}8$ $(\text{GeV}/c)^2$. The positions are independent of s for $s \to \infty$.

(3) The pp scattering amplitude at present energies should have a large real component in the neighborhood of the first minimum, $-t \sim 1\text{-}2$ $(\text{GeV}/c)^2$.

(4) At large values of $-t$ [$-t \sim 15$ $(\text{GeV}/c)^2$ for pp scattering], hadron scattering amplitudes should approach the product of form factors given in Eq. (II. 7). This result is consistent with the rigorous lower bounds on the cross section at fixed angles.[12] The empirical fits to the data suggested by Akerlof et al.[9] and Krisch[13] are not.

In contrast to the model of Abarbanel, Drell, and Gilman,[14] the present model predicts a predominantly imaginary scattering amplitude in this large-momentum-transfer region.

(5) Except for minor differences associated with charge exchange (isospin dependence of the absorption), the np and pp cross sections should be identical at high energies at forward angles. This statement perhaps requires explanation since the identification of charge and matter form factors obviously fails for the neutron. All types of hadronic matter presumably contribute to the absorption in hadron-hadron scattering. On the other hand, different types of matter may carry different electric charges, and hence contribute differently to electromagnetic form factors. The important features of the matter distribution for present purposes are its general extent and its smoothness properties. It seems quite likely that the charge and matter distributions of the proton are similar in these respects, but differences in detail are certainly to be expected. We expect also that the matter distributions of the neutron and proton are quite similar.

Complete measurements of $d\sigma/dt$ in pp scattering at the highest energies available, measurements of the rate of shrinkage of the cross sections at fixed t, and extended measurements of polarization in high-energy pp scattering would be especially useful as tests of the diffraction model. The physical ideas involved in the model are simple and appealing; however, it would be nice to obtain a deeper theoretical understanding of the model in a language more suitable to relativistic field theory.

REFERENCES

on

Application of Multi-Regge Theory to Production Processes

1. D. Amati, S. Fubini, and A. Stanghellini, Nuovo Cimento 26, 896 (1962).
   S. Fubini, lectures at Scottish Univ. Summer School (1963), ed. by R. Moorhouse.
2. S. Frautschi, Nuovo Cimento 28, 409 (1963).
3. T. W. B. Kibble, Phys. Rev. 131, 2282 (1963).
4. K. Ter-Martirosyan, Nuclear Physics 68, 591 (1965).
5. F. Zachariasen, G. Zweig, Phys. Rev. 160, 1322 (1967)
   Phys. Rev. 160, 1326 (1967).
6. T. W. B. Kibble, Phys. Rev. 117, 1159 (1960).
7. R. Dolen, D. Horn, C. Schmid, Phys. Rev. 166, 1768 (1968)
   L. A. P. Balazs, J. M. Cornwall, Phys. Rev. 160, 1313 (1967).
8. H. Harari, Phys. Rev. Letters 20, 1395 (1968).
   P. G. O. Freund, Phys. Rev. Letters 20, 235 (1968).
9. N. Byers, C. N. Yang, Rev. Mod. Phys. 36, 595 (1964).
10. P. Nyborg, et al., Phys. Rev. 140, B914 (1965).
11. Chan Hung-Mo, K. Kajantie, G. Ranft, Nuovo Cimento 49A, 157 (1967).
12. L. Durand, III, Phys. Rev., 154, 1537 (1967);
    R. P. Feynman (unpublished);
    L. Van Hove, Phys. Letters 24B, 183 (1967).

13. R. L. Sugar, J. D. Sullivan, Phys. Rev. 166, 1515 (1968); R. Blankenbecler, R. L. Sugar, Phys. Rev. 168, 1597 (1968).

14. S. C. Frautschi, L. M. Jones, Phys. Rev. 163, 1820 (1967) Phys. Rev. 167, 1335 (1968).

15. Chan Hong-Mo, J. Loskiewicz, and W. W. M. Allison, Nuovo Cimento 57A, 93 (1968); E. L. Berger, Phys. Rev. Letters 21, 701 (1968), and 20, 964 (1968), and Phys. Rev. 166, 1525 (1968); G. Alexander, A. Firestone, C. Fu, G. Goldhaber, and A. Pignotti, University of California Radiation Laboratory Report No. 18321, 1968 (unpublished).

16. N. F. Bali, G. F. Chew, A. Pignotti, Phys. Rev. Letters 19, 614 (1967).

17. S. B. Treiman, C. N. Young, Phys. Rev. Letters 8, 140 (1962).

18. An account of this work has been previously published: R. Lipes, G. Zweig, W. Robertson, Phys. Rev. Letters 22, 433 (1969).

19. Chan Hong-Mo, K. Kajantie, G. Ranft, W. Beusch, and E. Flaminio, Nuovo Cimento 51A, 696 (1967); S. Ratti, in Proceedings of the Topical Conference on High-Energy Collisions of Hadrons, CERN, 1968 (CERN Scientific Information Service, Geneva, Switzerland, 1968).

20. G. F. Chew and A. Pignotti, Phys. Rev. Letters 20, 1078 (1968).

21. R. Dolen, D. Horn, and C. Schmid, Phys. Rev. 166, 1768 (1968); R. Slansky, California Institute of Technology Report No. CALT-68-160, 1968 (unpublished).

22. More precisely, we require $(\pi^+ + p_f)^2 \geq (1.350\ \text{BeV})^2$, $(\pi^+ + \pi_f^-)^2 \neq (0.765 \pm 0.065\ \text{BeV})^2$, $(1.25 \pm 0.05\ \text{BeV})^2$.

23. The relative phase of the main term and the added correction cannot be distinguished from the relative absolute magnitudes of these two terms since the square of the correction term is negligible. Therefore we have essentially one degree of freedom in correcting our fits to the distributions.

24. The ρ signal continues to exist and dominate the f even when the $s_{\pi X}$ cut is increased from 2 to 3 BeV^2.

25. V. Barger, Topical Conference on High Energy Collisions of Hadrons, CERN, Geneva, 1968, Vol. I, p. 3.

26. M. Derrick, Topical Conference on High Energy Collisions of Hadrons, CERN, Geneva, 1968, Vol. I, p. 111.

27. V. Barger, D. Cline, Phys. Rev. Letters 19, 1504 (1967).

28. W. Rarita, R. J. Riddel, Jr., C. B. Chiu, R. J. N. Phillips, "Regge Pole Model for πp, pp, and $\bar{p}$p Scattering", UCRL Report - 17523 (1967).

29. L. Sertorio, M. Toller, Nuovo Cimento 33, 413 (1964).

30. M. Toller, Nuovo Cimento 37, 631 (1965).

31. V. Bargmann, Ann. Math. 48, 568 (1947).

32. N. F. Bali, G. F. Chew, A. Pignotti, Phys. Rev. 163, 1572 (1967).

33. T. L. Trueman, G. C. Wick, Ann. Phys. 26, 322 (1964).

34. G. Cohen-Tannondji, A. Morel, H. Navelet, Ann. Phys. 46, 239 (1968).

35. A. Capella, Nuovo Cimento 56A, 701 (1968).

36. G. Bros, H. Epstein, V. Glaser, Commun. Math. Phys. 1, 240 (1965).

37. K. Gottfried, J. D. Jackson, Nuovo Cimento 33, 309 (1964).

REFERENCES

on

High Energy Model for Proton-Proton Scattering

1. T. T. Wu and C. N. Yang, Phys. Rev. 137, B708 (1965).
2. N. Byers and C. N. Yang, Phys. Rev. 142, 976 (1966).
3. T. T. Chou and C. N. Yang, Phys. Rev. 170, 1591 (1968).
4. R. E. Taylor, Proceedings of the International Symposium on Electron and Photon Interactions at High Energies, Stanford, California, 1967, p. 78.
   D. H. Coward, et al., Phys. Rev. Letters 20, 292 (1968).
5. V. Barger, M. Olsson, D. Reeder, Nuclear Phys. B5, 411 (1968).
6. K. J. Foley et al., Phys. Rev. Letters 19, 857 (1967).
7. P. Grannis et al., Phys. Rev. 148, 1297 (1966).
8. N. E. Booth, et al., Phys. Rev. Letters 21, 651 (1968).
9. C. W. Akerlof et al., Phys. Rev. Letters 17, 1105 (1966), and Phys. Rev. 159, 1138 (1967); J. V. Allaby et al., Phys. Letters 25B, 156 (1967); J. V. Allaby, et al., Papers 605 (a), 605 (b) of 14th International Conference on High Energy Physics, Vienna, Austria, 1968.
10. K. J. Foley et al., Phys. Rev. Letters 10, 376 (1963); G. Cocconi et al., Phys. Rev. 138, B165 (1965).

11. T. L. Gervais and F. J. Yndurain, Phys. Rev. Letters 20, 27 (1968).

12. F. Cerulus and A. Martin, Phys. Letters 8, 80 (1964); T. Kinoshita, Phys. Rev. Letters 12, 257 (1964).

13. A. D. Krisch, Phys. Rev. Letters 19, 1149 (1967).

14. H. D. I. Abarbanel, S. D. Drell, and F. J. Gilman, Phys. Rev. Letters 20, 280 (1968).